Dinitrogen Rearranging over a Metal−Oxo Surface and Cleaving to Nitride: From the End-On to the Side-On Bonding Mode, to the Stepwise Cleavage of the N≡N Bonds Assisted by Nb^{III}-calix[4]arene

Alessandro Caselli,[†] Euro Solari,[†] Rosario Scopelliti,[†] Carlo Floriani,*[,†] Nazzareno Re,[‡] Corrado Rizzoli,[§] and Angiola Chiesi-Villa[§]

Contribution from the Institut de Chimie Minérale et Analytique, BCH, Université de Lausanne, CH-1015 Lausanne, Switzerland, Facoltà di Farmacia, Università degli Studi "G. D'Annunzio", I-66100 Chieti, Italy, and Dipartimento di Chimica, Università di Parma, I-43100 Parma, Italy

Received December 10, 1999

Abstract: Four-electron reduction of dinitrogen has been achieved in the reaction of N_2 with [{*p*-Bu^t-calix[4]-$(O)_4$}$_2$Nb$_2$(μ-M)$_2$] (M = Li, **3**; M = Na, **4**; M = K, **5**), which contain a very reactive Nb═Nb unit [Nb═Nb = 2.659(1) Å; **4**], in THF. The reaction leads to the dinuclear complexes [{*p*-Bu^t-calix[4]-$(O)_4$}$_2$(Nb≡N−N≡Nb)]$^{2-}$ M^+_2 (M = Li, **6**; M = Na, **7**; M = K, **8**) [Nb≡N = 1.747(12) Å, N−N = 1.390(17) Å; **7**], containing the hydrazido $[N_2]^{4-}$ anion. Two-electron reduction of the hydrazido tetraanion in **7** using sodium metal leads to the nitrido species **11**, [{*p*-Bu^t-calix[4]-$(O)_4$}$_2$Nb$_2$(μ-N)$_2$(μ-Na)$_2$Na$_2$], which in solution is in equilibrium with the monomeric form **18**, [{*p*-Bu^t-calix[4]-$(O)_4$}Nb≡N−NaS$_n$]. Two distinct pathways have been identified as a function of the solvent used (THF or DME). In the case of DME, the key intermediate **12** has been intercepted as green crystals. The formation of **12**, [{*p*-Bu^t-calix[4]-$(O)_4$}$_2$Nb$_2$(μ-η^2:η^2-N$_2$)(μ-Na)$_3$-Na], results from the reduction of Nb(V) to Nb(IV), which temporarily stores the two electrons in an Nb−Nb bond [N−N = 1.403(8) Å, Nb−Nb, 2.635(1) Å]. Complex **12** contains a μ-η^2:η^2 side-on N_2 group, bonded between two niobiums and preorganized to be transformed into two nitrido anions. Heating in pyridine (90 °C) converts **12** to **11**, with simultaneous cleavage of the Nb−Nb and N−N bonds, the heating causing two-electron transfer from the Nb−Nb to the N−N bond. The reaction of **4** with N_2, carried out in toluene instead of THF or DME, gives a nitrido complex, [{*p*-Bu^t-calix[4]-$(O)_4$}$_3$Nb$_3$(μ-N)$_2$Na$_3$(THF)$_2$], **15**, which can be formed equally well from the reaction of **4a** with **7a** carried out in a 1:2 molar ratio in toluene. Complex **15** breaks up in $CHCl_3$ or toluene, upon addition of TMEDA, into [{*p*-Bu^t-calix[4]-$(O)_4$}$_2$Nb$_2$(μ-N)$_2${μ-Na$_2$-(TMEDA)$_2$}Na$_2$], **16**, and [{*p*-Bu^t-calix[4]-$(O)_4$}$_2$Nb$_2$(μ-N)][Na(TMEDA)$_2$], **17**.

Introduction

Although transition metal complexes have long been used to mediate dinitrogen activation,[1] success has been limited almost exclusively to dinitrogen fixation and to two- and four-electron reductions of dinitrogen to diazenido[1,2] and hydrazido anions.[1,3] Six-electron reduction of dinitrogen to nitride or ammonia using well-defined transition metal complexes in a homogeneous phase is a quite rare event in two respects. The first one is the stoichiometric result per se, and the second is the understanding of the stepwise reaction pathway. A unique contribution to this area of dinitrogen activation is Cummins' work,[4] while a recent communication deals with a vanadium-assisted N≡N triple bond cleavage.[5] Our approach to this field of research, considering some major facets of the problem is reported in detail here. Preliminary results have been briefly communicated.[6]

* To whom correspondence should be addressed.
[†] Université de Lausanne.
[‡] Università degli Studi "G. D'Annunzia".
[§] Università di Parma.

(1) General reviews of transition metal dinitrogen complexes: (a) Allen, A. D.; Harris, R. O.; Loescher, B. R.; Stevens, J. R.; Whiteley, R. N. *Chem. Rev.* **1973**, *73*, 11. (b) Chatt, J.; Dilworth, J. R.; Richards, R. L. *Chem. Rev.* **1978**, *78*, 589. (c) Henderson, R. A.; Leigh, G. J.; Pickett, C. J. *Adv. Inorg. Chem. Radiochem.* **1983**, *27*, 197. (d) Leigh, G. J. *Acc. Chem. Res.* **1992**, *25*, 177. (e) Leigh, G. J. *New J. Chem.* **1994**, *18*, 157. (f) Hidai, M.; Mizobe, Y. *Chem. Rev.* **1995**, *95*, 1115. (g) Shilov, A. E. *Metal Complexes in Biomimetic Chemical Reactions*; CRC: Boca Raton, FL, 1997. (h) Tuczek, F. *Angew. Chem., Int. Ed. Engl.* **1998**, *37*, 2636.

(2) (a) Kol, M.; Schrock, R. R.; Kempe, R.; Davis, W. M. *J. Am. Chem. Soc.* **1994**, *116*, 4382. (b) O'Donoghue, M. B.; Zanetti, N. C.; Davis, W. M.; Schrock, R. R. *J. Am. Chem. Soc.* **1997**, *119*, 2753. (c) Shih, K.-Y.; Schrock, R. R.; Kempe, R. *J. Am. Chem. Soc.* **1994**, *116*, 8804. (d) Odom, A. L.; Arnold, P. L.; Cummins, C. C. *J. Am. Chem. Soc.* **1998**, *120*, 5836. (e) Campazzi, E.; Solari, E.; Floriani, C.; Scopelliti, R. *Chem. Commun.* **1998**, 2603. (f) Ferguson, R.; Solari, E.; Floriani, C.; Osella, D.; Ravera, M.; Re, N.; Chiesi-Villa, A.; Rizzoli, C. *J. Am. Chem. Soc.* **1997**, *119*, 10104. (g) O'Donoghue, M. B.; Davis, W. M.; Schrock, R. R. *Inorg. Chem.* **1998**, *37*, 5149. (h) O'Donoghue, M. B.; Davis, W. M.; Schrock, R. R.; Reiff, W. M. *Inorg. Chem.* **1999**, *38*, 243.

(3) (a) O'Regan, M. B.; Liu, A. H.; Finch, W. C.; Schrock, R. R.; Davis, W. M. *J. Am. Chem. Soc.* **1990**, *112*, 4331. (b) Basch, H.; Musaev, D. G.; Morokuma, K.; Fryzuk, M. D.; Love, J. B.; Seidel, W. W.; Albinati, A.; Koetzle, T. F.; Klooster, W. T.; Mason, S. A.; Eckert, J. *J. Am. Chem. Soc.* **1999**, *121*, 523. (c) Schrock, R. R.; Wesolek, M.; Liu, A. H.; Wallace, K. C.; Dewan, J. C. *Inorg. Chem.* **1988**, *27*, 2050. (d) Schrock, R. R.; Glassman, T. E.; Vale, M. G.; Kol, M. *J. Am. Chem. Soc.* **1993**, *115*, 1760. (e) Rocklage, S. M.; Schrock, R. R. *J. Am. Chem. Soc.* **1982**, *104*, 3077. (f) Rocklage, S. M.; Turner, H. W.; Fellmann, J. D.; Schrock, R. R. *Organometallics* **1982**, *1*, 703. (g) Turner, H. W.; Fellmann, J. D.; Rocklage, S. M.; Schrock, R. R.; Churchill, M. R.; Wasserman, H. J. *J. Am. Chem. Soc.* **1980**, *102*, 7809. (h) Churchill, M. R.; Li, Y.-J.; Theopold, K. H.; Schrock, R. R. *Inorg. Chem.* **1984**, *23*, 4472. (i) Schrock, R. R.; Kolodziej, R. M.; Liu, A. H.; Davis, W. M.; Vale, M. G. *J. Am. Chem. Soc.* **1990**, *112*, 4338. (j) Fryzuk, M. D.; Haddad, T. S.; Mylvaganam, M.; McConville, D. H.; Rettig, S. J. *J. Am. Chem. Soc.* **1993**, *115*, 2782.

(4) Laplaza, C. E.; Johnson, M. J. A.; Peters, J. C.; Odom, A. L.; Kim, E.; Cummins, C. C.; George, G. N.; Pickering, I. J. *J. Am. Chem. Soc.* **1996**, *118*, 8623 and references therein.

(5) Clentsmith, G. K. B.; Bates, V. M. E.; Hitchcock, P. B.; Cloke, F. G. N. *J. Am. Chem. Soc.* **1999**, *121*, 10444.

10.1021/ja9943288 CCC: $19.00
Published on Web 04/04/2000

Our attention was focused on (i) the stepwise supply of electrons to dinitrogen up to the complete cleavage of the N≡N triple bond, (ii) how dinitrogen binding two metal ions rearranges its bonding mode, thus being ready to cleave to nitride, (iii) the use of oxygen donor atoms preorganized in a configuration resembling that of a metal−oxo surface, and (iv) the relevance of the bifunctionality of the systems we have used. The bifunctional complexes contain an electron-rich metal, intended to provide electrons to the substrate, and a Lewis acid center. The role of the latter, which in our case is an alkali metal cation, is not only to participate to the binding and/or polarization of the substrate but also to affect the thermodynamics of the overall reaction, with a major contribution derived from the solvation of this cation. As a matter of fact, we were able to select the four- or the six-electron reduction pathway of dinitrogen by the use of an appropriate solvent. The nature of the solvent allowed the interception of intermediates in the transformation of the four-electron-reduced N_2 into nitride.

At this point, the original contribution by the Shilov group[7] to the area of dinitrogen reduction using bifunctional systems should be mentioned. This approach, dating back 30 years, was based on the use of a heterogeneous mixture of a low-valence early transition metal hydroxide and magnesium hydroxide. Our approach can be viewed as, among other things, the attempt to transfer the input from Shilov's work into a homogeneous phase at a molecular level to understand how the system works.

The present report describes our reduction of dinitrogen to nitride using as the active species an Nb^{III}-calix[4]arene[8] dimer containing a very reactive Nb═Nb double bond.[9] We were successful not only in producing metal−nitrido species from a well-defined dinitrogen complex following different pathways but also in singling out key intermediates along these pathways.

Experimental Section

All operations were carried out under an atmosphere of purified nitrogen. All solvents were purified by standard methods and freshly distilled prior to use. IR spectra were recorded on a Perkin-Elmer FT 1600 spectrophotometer. Magnetic susceptibilities were measured at 80−300 K on an MPMS5 SQUID susceptometer (Quantum Design) operating at a magnetic field strength of 3 kOe. ^{1}H NMR spectra were recorded on 200-AC and DPX-400 Bruker instruments. ^{15}N NMR and ^{7}Li NMR spectra were recorded on a DPX-400 Bruker instrument referenced to internal nitromethane (sealed capillary tube)[10] and to external LiCl, respectively, set at 0 ppm. Abbreviations: DME = dimethoxyethane; TDF = perdeuterated THF.

Synthesis of 1. $NbCl_5$ (18.18 g, 67.30 mmol) was added to a toluene (500 mL) suspension of *p*-Bu^t-calix[4]arene·CH_2Cl_2[11] (49.39 g, 67.30 mmol), and the resulting red mixture was refluxed for 16 h. (N.B.: Evolution of HCl occurred). The solvent was removed in vacuo, fresh toluene was added (500 mL), stirring was maintained for 20 min, and the solvent was then evaporated to dryness again. Complex **1** was collected from toluene (500 mL) as a red powder (58.65 g, 98%). Anal. Calcd for **1**·2.6C_7H_8, $C_{106.2}H_{124.8}Cl_2Nb_2O_8$: C, 71.44; H, 7.04. Found: C, 71.00; H, 7.08. ^{1}H NMR (CD_2Cl_2, 298 K; ppm): δ 7.17 (s, 8H, Ar H) overlapping with 7.12−7.22 (m, 13H, toluene), 7.12 (s, 8H, Ar H), 5.07 (d, 4H, J = 12.5 Hz, endo CH_2), 4.62 (d, 4H, J = 13.6 Hz, endo CH_2), 3.51 (d, 4H, J = 12.5 Hz, exo CH_2), 3.36 (d, 4H, J = 13.6 Hz, exo CH_2), 2.34 (s, 7.8H, toluene), 1.33 (s, 18H, Bu^t), 1.22 (s, 36H, Bu^t), 1.17 (s, 18H, Bu^t). The product is almost insoluble in hydrocarbons and THF, slightly soluble in chlorinated solvents, and thermally stable.

Synthesis of 2. Sodium (1.422 g, 61.85 mmol) and naphthalene (0.340 g, 2.65 mmol) were added to a red THF (500 mL) suspension of **1**·2.6C_7H_8 (55.40 g, 31.02 mmol), and the reaction mixture was stirred at room temperature. After 3 days, the sodium was consumed, and the resulting brown suspension was extracted with the mother liquors for 48 h, the volume was concentrated to 100 mL, and the solid was filtered off and dried in vacuo, giving **2** as a microcrystalline light brown powder (47.54 g, 87%). Anal. Calcd for **2**·4THF, $C_{104}H_{136}Nb_2O_{12}$: C, 70.81; H, 7.77. Found: C, 70.83; H, 8.10. ^{1}H NMR (CD_2Cl_2, 298 K; ppm): δ 7.32 (s, 4H, Ar H), 7.22 (s, 4H, Ar H), 7.16 (s, 4H, Ar H), 7.07 (s, 4H, Ar H), 4.52 (d, 4H, J = 13.1 Hz, endo CH_2), 4.40 (d, 4H, J = 12.0 Hz, endo CH_2), 3.67 (m, 16H, THF), 3.57 (d, 4H, J = 13.1 Hz, exo CH_2), 3.36 (d, 4H, J = 12.0 Hz, exo CH_2), 1.81 (m, 16H, THF), 1.28 (s, 18H, Bu^t), 1.24 (s, 36H, Bu^t), 1.15 (s, 18H, Bu^t). The product was not stable in CD_2Cl_2, yielding **1** in ∼1 h. ^{1}H NMR (DMSO-d_6, 298 K; ppm): δ 7.11 (s, 4H, Ar H), 7.02 (s, 4H, Ar H), 6.95 (s, 8H, Ar H), 4.42 (m, 6H, endo CH_2) overlapping with 4.41 (d, 2H, J = 11.6 Hz, endo CH_2), 3.60 (m, 16H, THF), 3.16 (m, 6H, exo CH_2), 3.01 (d, 2H, J = 11.6 Hz, exo CH_2), 1.75 (m, 16H, THF), 1.16 (s, 18H, Bu^t), 1.13 (s, 36H, Bu^t), 1.12 (s, 18H, Bu^t). The product is thermally stable and slightly soluble in THF, hydrocarbons, and chlorinated solvents. Crystals were grown in a THF solution.

Synthesis of 3. The complex **2**·4THF (34.36 g, 19.48 mmol) was added to a freshly prepared THF (250 mL) suspension of lithium (0.267 g, 38.47 mmol) and naphthalene (0.17 g, 1.30 mmol) under an argon atmosphere. The reaction mixture was stirred for 6 days, after which the resulting brown suspension was extracted with mother liquors, the solvent was removed in vacuo, *n*-pentane (250 mL) was added to the residue, and complex **3** was collected as a brown solid (31.51 g, 79%). Anal. Calcd for **3**, $C_{120}H_{168}Li_2Nb_2O_{16}$: C, 69.75; H, 8.20. Found: C, 69.54; H, 8.17. ^{1}H NMR (C_4D_8O, 298 K; ppm): δ 7.10 (s, 8H, Ar H), 6.96 (s, 8H, Ar H), 5.00 (d, 8H, J = 12.0 Hz, endo CH_2), 3.62 (m, 32H, THF), 3.14 (d, 8H, J = 12.0 Hz, exo CH_2), 1.77 (m, 32H, THF), 1.26 (s, 36H, Bu^t), 1.10 (s, 36H, Bu^t). ^{7}Li NMR (C_4D_8O, 155.51 MHz, 298 K; ppm): δ −0.04 (s, Li). ^{1}H NMR (toluene-d_8, 298 K; ppm): δ 7.40 (s, 8H, Ar H), 7.04 (s, 8H, Ar H), 5.15 (d, 8H, J = 11.7 Hz, endo CH_2), 3.45 (m, 32H, THF) overlapping with 3.45 (d, 8H, exo CH_2), 1.50 (s, 36H, Bu^t), 1.34 (m, 32H, THF), 0.85 (s, 36H, Bu^t). ^{7}Li NMR (toluene-d_8, 155.51 MHz, 298 K; ppm): δ 0.94 (s, Li). Complex **3** is soluble in aromatic hydrocarbons and very soluble in THF. The temperature dependence of the magnetic moment of **3** shows a small residual paramagnetism, due to a high temperature-independent paramagnetism[12] (TIP) of 4×10^{-5} emu.

Synthesis of 4a and 4b. Sodium (0.616 g, 26.78 mmol) was added to a THF (300 mL) suspension of **2**·4THF (23.62 g, 13.39 mmol) under an argon atmosphere. The reaction mixture was stirred for 2 days, the

(6) Zanotti-Gerosa, A.; Solari, E.; Giannini, L.; Floriani, C.; Chiesi-Villa, A.; Rizzoli, C. *J. Am. Chem. Soc.* **1998**, *120*, 437.

(7) (a) Denisov, N. T.; Efimov, O. N.; Shuvalova, N. I.; Shilova, A. K.; Shilov, A. E. *Zh. Fiz. Khim.* **1970**, *44*, 2694. (b) Shilov, A. E.; Denisov, D. N.; Efimov, O. N.; Shuvalov, N. F.; Shuvalova, N. I.; Shilova, E. *Nature* (London) **1971**, *231*, 460. (c) Shilov, A. E. In *Perspectives in Coordination Chemistry*; Williams, A. F., Floriani, C., Merbach, A. E., Eds.; VCHA: Basel, Switzerland, 1992; pp 233−244 and references therein. (d) Shilov, A. E. *Pure Appl. Chem.* **1992**, *64*, 1409. (e) Shilov, A. E. *New J. Chem.* **1992**, *16*, 213. (f) Antipin, M. Yu.; Struchkov, Yu. T.; Shilov, A. E.; Shilova, A. K. *Gazz. Chim. Ital.* **1993**, *123*, 265. (g) Antipin, M. Yu.; Didenko, L. P.; Kachapina, L. M.; Shilov, A. E.; Shilova, A. K.; Struchkov, Yu. T. *J. Chem. Soc., Chem. Commun.* **1989**, 1467. (h) Luneva, N. P.; Mironova, S. A.; Shilov, A. E.; Antipin, M. Yu.; Struchkov, Yu. T. *Angew. Chem., Int. Ed. Engl.* **1993**, *32*, 1178.

(8) Organometallic chemistry based on the calix[4]arene skeleton: (a) Giannini, L.; Dovesi, S.; Solari, E.; Floriani, C.; Chiesi-Villa, A.; Rizzoli, C. *Angew. Chem., Int. Ed. Engl.* **1999**, *38*, 807. (b) Giannini, L.; Guillemot, G.; Solari, E.; Floriani, C.; Re, N.; Chiesi-Villa, A.; Rizzoli, C. *J. Am. Chem. Soc.* **1999**, *121*, 2797 and 2784. (c) Giannini, L.; Solari, E.; Dovesi, S.; Floriani, C.; Re, N.; Chiesi-Villa, A.; Rizzoli, C. *J. Am. Chem. Soc.* **1999**, *121*, 2784. (d) Castellano, B.; Solari, E.; Floriani, C.; Re, N.; Chiesi-Villa, A.; Rizzoli, C. *Chem.−Eur. J.* **1999**, *5*, 722. (e) Floriani, C. *Chem.−Eur. J.* **1999**, *5*, 19. (f) Castellano, B.; Solari, E.; Floriani, C.; Re, N.; Chiesi-Villa, A.; Rizzoli, C. *Organometallics* **1998**, *17*, 2328. (g) Giannini, L.; Caselli, A.; Solari, E.; Floriani, C.; Chiesi-Villa, A.; Rizzoli, C.; Re, N.; Sgamellotti, A. *J. Am. Chem. Soc.* **1997**, *119*, 9709 and 9198.

(9) Metal−metal bonds in metallacalix[4]arene chemistry: Giannini, L.; Solari, E.; Floriani, C.; Re, N.; Chiesi-Villa, A.; Rizzoli, C. *Inorg. Chem.* **1999**, *38*, 1438 and references therein.

(10) Reviews of ^{15}N NMR spectroscopy: (a) von Philipsborn, W.; Müller, R. *Angew. Chem., Int. Ed. Engl.* **1986**, *25*, 383. (b) Donovan-Mtunzi, S.; Richards, R. L.; Mason, J. *J. Chem. Soc., Dalton Trans.* **1984**, 1329.

(11) Arduini, A.; Casnati, A. In *Macrocycle Synthesis*; Parker, O., Ed.; Oxford University Press: New York, 1996; Chapter 7.

(12) Kahn, O. *Molecular Magnetism*; VCH: New York, 1992.

resulting turbid brown solution was filtered, and the solvent was removed in vacuo. *n*-Hexane (100 mL) was added to the residue, and **4a** was collected as a green powder (20.48 g, 78%). Anal. Calcd for **4a**, $C_{112}H_{152}Na_2Nb_2O_{14}$: C, 68.84; H, 7.84. Found: C, 68.92; H, 7.65. ^{1}H NMR (C_4D_8O, 298 K; ppm): δ 7.04 (s, 16H, Ar H), 4.82 (d, 8H, $J = 12.00$ Hz, endo CH_2), 3.62 (m, 24H, THF), 3.13 (d, 8H, $J = 12.00$ Hz, exo CH_2), 1.77 (m, 24H, THF), 1.19 (s, 72H, Bu^t). ^{1}H NMR (C_7H_8, 233 K; ppm): δ 7.54 (s, 8H, Ar H), 7.21 (s, 8H, Ar H), 5.19 (d, 8H, $J = 11.2$ Hz, endo CH_2), 3.45 (d, 8H, $J = 11.2$ Hz, exo CH_2), 3.30 (m, 24H, THF), 1.62 (s, 36H, Bu^t), 1.21 (s, 24H, THF), 1.00 (s, 36H, Bu^t). The product is very soluble in THF, soluble in toluene, and slightly soluble in DME, Et_2O, and alkanes. Crystals suitable for X-ray analysis were obtained from a saturated DME/toluene solution under an argon atmosphere (**4b**·$6C_7H_8$). Compound **4a** is thermally and photochemically stable in THF solutions.

Synthesis of 5. Potassium (0.38 g, 9.72 mmol) was added to a THF (150 mL) suspension of **2**·4THF (8.48 g, 4.81 mmol) under an argon atmosphere and the reaction mixture was stirred for 24 h. The resulting dark purple suspension was filtered, the solvent was removed in vacuo, *n*-pentane (90 mL) was added to the residue, and **5** was collected as a green solid (6.46 g, 68%). Anal. Calcd for **5**, $C_{112}H_{152}K_2Nb_2O_{14}$: C, 67.72; H, 7.71. Found: C, 67.72; H, 7.42.

Synthesis of 6a. A THF (80 mL) solution of **3** (2.55 g, 1.23 mmol), prepared under an argon atmosphere, was saturated with N_2. The reaction mixture was stirred for 10 days, after which the solvent was removed in vacuo from the resulting reddish solution, *n*-pentane (30 mL) was added, and **6a** was collected as a yellow solid (1.87 g, 73%). Anal. Calcd for **6a**, $C_{120}H_{168}Li_2N_2Nb_2O_{16}$: C, 68.82; H, 8.09; N, 1.34. Found: C, 68.41; H, 7.73; N, 1.09. ^{1}H NMR (C_4D_8O, 298 K; ppm): δ 7.00 (s, 16H, Ar H), 4.71 (d, 8H, $J = 11.6$ Hz, endo CH_2), 3.62 (m, 32H, THF), 3.09 (d, 8H, $J = 11.6$ Hz, exo CH_2), 1.77 (m, 32H, THF), 1.18 (s, 72H, Bu^t). ^{7}Li NMR (C_4D_8O, 155.51 MHz, 298 K; ppm): δ −2.14 (s, Li). ^{1}H NMR (C_5D_5N, 298 K; ppm): δ 7.09 (s, 16H, Ar H), 4.77 (d, 8H, $J = 11.6$ Hz, endo CH_2), 3.64 (m, 32H, THF), 3.07 (d, 8H, $J = 11.6$ Hz, exo CH_2), 1.60 (m, 32H, THF), 1.14 (s, 72H, Bu^t). When a toluene solution of **3** was treated with N_2, no reaction occurred.

Synthesis of 6b. LiCl (0.216 g, 5.10 mmol) was added to a THF (250 mL) solution of **7a** (5.02 g, 2.54 mmol), yielding a turbid yellow solution. The reaction mixture was stirred for 20 min and then filtered to give a clear yellow solution. The solvent was removed in vacuo, DME (60 mL) was added, and **6b** was collected as a yellow solid (3.13 g, 55%). Anal. Calcd for **6b**, $C_{120}H_{184}Li_2N_2Nb_2O_{24}$: C, 64.39; H, 8.29; N, 1.25. Found: C, 64.00; H, 8.16; N, 1.25. ^{1}H NMR (C_5D_5N, 298 K; ppm): δ 7.09 (s, 16H, Ar H), 4.78 (d, 8H, $J = 11.6$ Hz, endo CH_2), 3.47 (s, 32H, DME), 3.25 (s, 48H, DME), 3.08 (d, 8H, $J = 11.6$ Hz, exo CH_2), 1.14 (s, 72H, Bu^t).

Synthesis of 7a−c. Sodium (0.919 g, 40.00 mmol) was added to a THF (300 mL) suspension of **2**·4THF (35.28 g, 20.00 mmol) under an argon atmosphere. The reaction mixture was stirred for 2 days, the resulting turbid brown solution was filtered, argon was replaced with nitrogen, vigorous stirring was maintained for 2 days, and the solvent was removed in vacuo. *n*-Hexane (200 mL) was added to the residue, and **7a** was collected as a yellow powder (30.44 g, 77%). Anal. Calcd for **7a**, $C_{112}H_{152}N_2Na_2Nb_2O_{14}$: C, 67.86; H, 7.73; N, 1.41. Found: C, 67.96; H, 7.73; N, 1.59. ^{1}H NMR (C_5D_5N, 298 K; ppm): δ 7.14 (s, 16H, Ar H), 4.89 (d, 8H, $J = 12.00$ Hz, endo CH_2), 3.64 (m, 24H, THF), 3.12 (d, 8H, $J = 12.00$ Hz, exo CH_2), 1.60 (m, 24H, THF), 1.14 (s, 72H, Bu^t). Raman (ν_{N-N}, solid state): 1372 cm^{-1}. The same product (**7a**) could be obtained by dissolving **4a** in THF and stirring the resulting solution under a nitrogen atmosphere. [{Nb}$_2{}^{15}N_2$]Na_2·6THF was prepared by dissolving **4a** (9.117 g, 4.66 mmol) in THF (125 mL) and stirring the resulting solution under a $^{15}N_2$ atmosphere (>98% isotropic purity; purchased from Cambridge Isotopes Laboratory). Workup was carried out under an unlabeled N_2 atmosphere. ^{15}N NMR (C_5H_5N, 40.556 MHz, 298 K; ppm): δ −4.115. Raman ($\nu^{15}{}_{N-}{}^{15}{}_N$, solid state): 1328 cm^{-1}. Compound **7b** could be obtained as yellow crystals in good yield (67%) by washing the product twice with DME instead of *n*-hexane. Anal. Calcd for **7b**, $C_{116}H_{174}N_2Na_2Nb_2O_{22}$: C, 63.90; H, 8.04; N, 1.28. Found: C, 64.09; H, 8.05; N, 1.13. ^{1}H NMR (C_5D_5N, 298 K; ppm): δ 7.14 (s, 16H, Ar H), 4.88 (d, 8H, $J = 12.0$ Hz, endo CH_2), 3.48 (s, 28H, DME), 3.26 (s, 42H, DME), 3.13 (d, 8H, $J = 12.0$ Hz, exo CH_2), 1.15 (s, 72H, Bu^t). Recrystallization of **7a** from diglyme/benzene gave **7c**·$2C_6H_6$ as crystals suitable for the X-ray analysis. **7a** is soluble in aromatic hydrocarbons, slightly soluble in THF, and almost insoluble in DME. **7b** is extremely soluble in THF and soluble in aromatic hydrocarbons. Solutions of **7a** and **7b** are stable to temperature and solar light. Under no circumstance was loss of N_2 observed. In a gas-volumetric experiment, **4a** (1.557 g, 0.797 mmol), dissolved in THF (125 mL), at 288 K and 1 atm absorbed 0.7 mmol of N_2 in 30 h.

Synthesis of 7d. A THF solution of 18-crown-6-ether (0.025 M, 1.61 mmol) was added dropwise to a THF (150 mL) solution of **7a** (1.41 g, 0.71 mmol) with vigorous stirring. The light yellow crystalline solid that precipitated was filtered off and dried in vacuo (1.40 g, 79%). Anal. Calcd for **7d**, $C_{136}H_{200}N_2Na_2Nb_2O_{26}$: C, 65.06; H, 8.04; N, 1.12. Found: C, 65.27; H, 8.37; N, 0.96. ^{1}H NMR (C_5D_5N, 298 K; ppm): δ 7.27 (s, 16H, Ar H), 5.41 (d, 8H, $J = 11.7$ Hz, endo CH_2), 3.63 (s, 24H, THF), 3.38 (s, 48H, 18-crown-6-ether) overlapping with 3.40 (d, 8H, $J = 11.7$ Hz, exo CH_2), 1.60 (s, 24H, THF), 1.20 (s, 72H, Bu^t).

Synthesis of 8a. A THF (100 mL) solution of **5** (3.17 g, 1.60 mmol) was saturated with N_2, and the mixture was stirred for 3 days. The solvent was evaporated, *n*-pentane (30 mL) was added to the residue, and **8a** along with some impurities was collected as a yellowish solid (1.77 g, 51%). Anal. Calcd for **8a**, $C_{120}H_{168}K_2N_2Nb_2O_{16}$: C, 66.77; H, 7.84; N, 1.30. Found: C, 65.19; H, 7.83; N, 1.13. ^{1}H NMR (C_5D_5N, 253 K; ppm): δ 7.43 (s, 4H, Ar H), 7.21 (s, 4H, Ar H), 7.13 (s, 4H, Ar H), 7.02 (s, 4H, Ar H), 5.11 (d, 4H, $J = 12.8$ Hz, endo CH_2), 4.39 (d, 4H, $J = 13.2$ Hz, endo CH_2), 3.64 (m, 32H, THF), 3.40 (m, 8H, exo CH_2), 1.60 (m, 32H, THF), 1.46 (s, 18H, Bu^t), 1.24 (s, 18H, Bu^t), 0.68 (s, 36H, Bu^t).

Synthesis of 8b. In a 1 L flask, potassium (0.306 g, 7.83 mmol) was added to a cooled (−40 °C) THF (200 mL) suspension of **2**·4THF (7.02 g, 3.98 mmol) under a nitrogen atmosphere. The reaction mixture was stirred for 24 h at −40 °C and then was allowed to reach room temperature over a 3 day period with vigorous stirring. The solvent was evaporated from the resulting reddish suspension, DME (150 mL) was added to the residue, and **8b** was collected as a yellow solid (1.92 g, 21%). Anal. Calcd for **8b**, $C_{120}H_{184}K_2N_2Nb_2O_{24}$: C, 62.59; H, 8.05; N, 1.22. Found: C, 62.46; H, 7.88; N, 1.27. ^{1}H NMR (C_5D_5N, 253 K; ppm): δ 7.43 (s, 4H, Ar H), 7.21 (s, 4H, Ar H), 7.13 (s, 4H, Ar H), 7.02 (s, 4H, Ar H), 5.11 (d, 4H, $J = 12.8$ Hz, endo CH_2), 4.39 (d, 4H, $J = 13.2$ Hz, endo CH_2), 3.40 (m, 32H, DME) overlapping with 3.40 (m, 8H, exo CH_2), 3.18 (m, 48H, DME), 1.46 (s, 18H, Bu^t), 1.24 (s, 18H, Bu^t), 0.68 (s, 36H, Bu^t).

Synthesis of 9a. Bu^{t}CN (0.344 g, 4.14 mmol) was added to a yellow THF (150 mL) suspension of **7a** (4.10 g, 2.07 mmol), yielding an orange solution. The reaction mixture was stirred for 10 h, whereupon a yellow precipitate appeared. Volatiles were removed in vacuo, and *n*-hexane (50 mL) was added to the yellow residue, which was then collected and dried in vacuo, giving **9a** as a yellow powder (3.44 g, 77%). Anal. Calcd for **9a**, $C_{122}H_{170}N_4Na_2Nb_2O_{14}$: C, 68.20; H, 7.98; N, 2.61. Found: C, 68.26; H, 8.03; N, 2.61. IR (Nujol; ν_{max}/cm^{-1}): 2205.8 (m). ^{1}H NMR (C_6D_6, 298 K; ppm): δ 7.19 (s, 16H, Ar H), 5.09 (d, 8H, $J = 12.0$ Hz, endo CH_2), 3.59 (m, 24H, THF), 3.41 (d, 8H, $J = 12$ Hz, exo CH_2), 1.34 (m, 24H, THF) overlapping with 1.31 (s, 72H, Bu^t), −0.10 (s, 18H, Bu^{t}CN). Raman (ν_{N-N}, solid state): 1348 cm^{-1}. Crystals were grown in diglyme/toluene solution (**9b**).

Reaction of 7a with PhCHO: Synthesis of 10. Benzaldehyde (0.376 g, 3.54 mmol) was added to a yellow THF (100 mL) solution of **7a** (3.65 g, 1.84 mmol). The reaction mixture, which darkened immediately, was stored at −20 °C for 24 h, and white **10** was collected as a microcrystalline solid (3.43 g, 88%). Anal. Calcd for **10**, $C_{60}H_{84}NaNbO_9$: C, 67.65; H, 7.95. Found: C, 67.30; H, 8.17. ^{1}H NMR (C_6D_6, 298 K; ppm): δ 7.10 (s, 8H, Ar H), 5.05 (d, $J = 12.2$ Hz, 4H, endo CH_2), 3.66 (m, 16H, THF), 3.38 (d, $J = 12.2$ Hz, 4H, exo CH_2), 1.38 (m, 16H, THF), 1.11 (s, 36H, Bu^t). ^{1}H NMR (py-d_5, 298 K; ppm): δ 7.27 (s, 8H, Ar H), 5.25 (d, $J = 11.7$ Hz, 4H, endo CH_2), 3.64 (m, 16H, THF), 3.38 (d, $J = 11.7$ Hz, 4H, exo CH_2), 1.59 (m, 16H, THF), 1.20 (s, 36H, Bu^t). The mother liquors were evaporated to dryness, the yellowish residue was washed with diethyl ether (30 mL), and PhCHNNCHPh was collected (0.25 g, 68%). ^{1}H NMR (C_6D_6): δ 8.69 (s, 2H, CH), 7.77 (m, 4H, Ar H), 7.08 (m, 6H, Ar H).

Synthesis of 11a and 11b. Sodium (0.330 g, 14.35 mmol) was added

to a THF (250 mL) amber-brown suspension of **7a** (14.46 g, 7.295 mmol), and the reaction mixture was stirred at room temperature for 5 days, yielding a black solution from which a white crystalline solid precipitated. The solid was extracted with the mother liquor during a period of 24 h, and the solution was concentrated to 50 mL. Cooling at room temperature resulted in the precipitation of **11a** as white crystals, which were collected and dried in vacuo (8.96 g, 51%). Anal. Calcd for **11a**, $C_{136}H_{200}N_2Na_4Nb_2O_{20}$: C, 66.38; H, 8.19; N, 1.14. Found: C, 65.92; H, 8.27; N, 1.13. The same product could be isolated by carrying out all the operations under an argon atmosphere, ruling out the hypothesis that atmospheric N_2 could be involved in the reaction. ^{1}H NMR (C_5D_5N, 298 K; ppm): δ 7.01 (s, 16H, Ar H), 5.29 (d, 8H, J = 11.7 Hz, endo CH_2), 3.64 (m, 48H, THF), 3.13 (d, 8H, J = 11.7 Hz, exo CH_2), 1.60 (m, 48H, THF), 1.12 (s, 72H, Bu^t). ^{1}H NMR (C_4D_8O, 298 K; ppm): δ 6.86 (s, 16H, Ar H), 4.92 (d, J = 11.6 Hz, 8H, endo CH_2), 3.61 (m, 48H, THF), 2.95 (d, J = 11.6 Hz, 8H, exo CH_2), 1.76 (m, 48 H, THF), 1.14 (s, 72H, Bu^t). [{Nb}$_2{}^{15}N_2Na_4(THF)_2$] was prepared by reducing isotopically labeled **7a**. Workup was carried out under an unlabeled N_2 atmosphere. ^{15}N NMR (C_5H_5N, 40.46 MHz, 298 K; ppm): δ 269.38. ^{15}N NMR (C_4H_8O, 40.56 MHz, 193 K; ppm): δ 278.9. The apparent C_{4v} symmetry remained unchanged at low temperature (−80 °C, THF). Crystals suitable for X-ray analysis were grown from a saturated DME/chlorobenzene solution (**11b**·$6C_6H_5Cl$). ^{1}H NMR analysis of the crude solid showed that, along with **11a**, small amounts of other diamagnetic products of very low symmetry were formed. Clean **11a** could be obtained in ≅40% yield via reduction with sodium naphthalenide in THF (at −30 °C the reaction was complete within 30 min). **11a** is slightly soluble in THF and DME and soluble in py. Solutions of **11a** are stable to the heat and solar light.

Synthesis of 11c. A greenish pyridine (25 mL) solution of **12** (0.62 g, 0.32 mmol), heated to 90 °C overnight, gave a reddish suspension. Volatiles were removed in vacuo, *n*-pentane (30 mL) was added to the residue, and **11c** was collected as a whitish solid (0.35 g, 43%). Anal. Calcd for **11c**, $C_{108}H_{124}N_6Na_4Nb_2O_8$: C, 67.85; H, 6.54; N, 4.40. Found: C, 66.50; H, 6.89; N, 4.14. ^{1}H NMR (C_5D_5N, 298 K; ppm): δ 7.01 (s, 16H, Ar H), 5.29 (d, 8H, J = 11.7 Hz, endo CH_2), 3.13 (d, 8H, J = 11.7 Hz, exo CH_2), 1.12 (s, 72H, Bu^t). The same reaction carried out in THF led only to decomposition products.

Synthesis of 12a and 12b. Sodium (0.34 g, 14.79 mmol) was added to a yellow DME (500 mL) suspension of **7b** (16.61 g, 7.62 mmol), and the reaction mixture was stirred at room temperature for 6 days, yielding a black suspension from which a white crystalline solid precipitated. ^{1}H NMR (py-d_5) analysis of the crude solid showed [Nb]$_2$-$(N)_2Na_4$ and [CalixNb]$_2$(μ-η^2:η^2-N_2)Na_4 as the only products detectable. The solid and the solution were separated by filtration, **11b**·3DME being collected as microcrystals (1.76 g, 10%). Anal. Calcd for $C_{116}H_{174}N_2$-$Na_4Nb_2O_{22}$: C, 62.58; H, 7.88; N, 1.26. Found: C, 62.84; H, 7.59; N, 1.01. ^{1}H NMR (C_5D_5N, 298 K; ppm): δ 7.02 (s, 16H, Ar H), 5.30 (d, 8H, J = 11.7 Hz, endo CH_2), 3.48 (s, 28H, DME), 3.25 (s, 42H, DME), 3.13 (d, 8H, J = 11.7 Hz, exo CH_2), 1.12 (s, 72H, Bu^t). Volatiles were removed from the solution, and *n*-pentane (150 mL) was added to the greenish residue. From the resulting turbid yellow solution a green solid precipitated after 20 min of stirring. The reaction mixture was stored for 24 h at −24 °C, and **12a** was collected as a green solid (7.47 g, 50%). Anal. Calcd for **12a**, $C_{104}H_{144}N_2Na_4Nb_2O_{16}$: C, 63.86; H, 7.42; N, 1.43. Found: C, 63.85; H, 7.61; N, 1.27. ^{1}H NMR (C_5D_5N, 298 K; ppm): δ 7.46 (s, 2H, Ar H), 7.23 (m, 2H, Ar H), 7.15 (s, 2H, Ar H), 7.10 (m, 2H, Ar H), 7.04 (b s, 6H, Ar H), 6.96 (s, 2H, Ar H), 5.61 (d, 2H, J = 12.0 Hz, endo CH_2), 5.42 (d, 2H, J = 12.0 Hz, endo CH_2), 5.32 (d, 2H, J = 12.8 Hz, endo CH_2), 5.16 (d, 2H, J = 11.2 Hz, endo CH_2), 3.48 (s, 16H, DME) overlapping with 3.45 (2H, exo CH_2), 3.25 (s, 24H, DME) overlapping with 3.25−3.09 (6H, exo CH_2), 1.48 (s, 9H, Bu^t), 1.38 (b s, 18H, Bu^t), 1.37 (s, 9H, Bu^t), 1.05 (s, 9H, Bu^t), 1.04 (s, 9H, Bu^t), 0.83 (b s, 18H, Bu^t). ^{15}N NMR (C_5H_5N, 40.56 MHz, 298 K; ppm): δ −30.6 Hz. Complex **12a**, when heated in a sealed tube in C_5D_5N to 90 °C for 24 h, gave clean **11c**. Complex **12a** is not thermally stable and is very soluble in aromatic hydrocarbons, py, THF, and DME. Crystals suitable for X-ray analysis were grown in a DME/*n*-hexane solution (**12b**·$5C_4H_{10}O_2$).

Synthesis of 13a and 13b. Pyridine *N*-oxide (0.034 g, 0.358 mmol) was added to a brown THF (100 mL) solution of **12a** (0.716 g, 0.366 mmol), yielding a reddish solution. Volatiles were removed in vacuo, and *n*-pentane (30 mL) was added. Complex **13a** was collected as a brick-red powder (0.180 g, 24%). Anal. Calcd for **13a**, $C_{109}H_{145}N_3Na_4$-Nb_2O_{15}: C, 64.97; H, 7.25; N, 2.09. Found: C, 65.21; H, 7.15; N, 2.10. ^{1}H NMR (C_5D_5N, 298 K; ppm): δ 8.34 (m, 2H, Ar H), 7.44 (m, 2H, Ar H), 7.35 (m, 2H, Ar H), 7.08 (m, 4H, Ar H), 7.02 (m, 2H, Ar H), 6.97 (m, 2H, Ar H), 6.92 (m, 2H, Ar H), 5.40 (d, 2H, J = 12.0 Hz, endo CH_2), 5.26 (d, 2H, J = 12.0 Hz, endo CH_2), 5.05 (d, 2H, J = 12.0 Hz, endo CH_2) overlapping with 5.03 (d, 2H, J = 12.0 Hz, endo CH_2), 3.64 (m, 8H, THF), 3.48 (s, 8H, DME), 3.34 (d, 2H, J = 12.0 Hz, exo CH_2), 3.25 (s, 12H, DME), 3.12 (d, 2H, J = 12.0 Hz, exo CH_2), 2.99 (d, 2H, J = 12.0 Hz, exo CH_2), 2.93 (d, 2H, J = 12.0 Hz, exo CH_2), 1.60 (m, 8H, THF), 1.47 (s, 18H, Bu^t), 1.30 (s, 18H, Bu^t), 0.86 (s, 18H, Bu^t), 0.83 (s, 18H, Bu^t). The amount of pyridine was calculated from the elemental analysis. Crystals suitable for X-ray analysis were grown in a DME solution (**13b**·2DME).

Synthesis of 14a and 14b. A sealed vial of **12a** under a nitrogen atmosphere was heated to 140 °C over 12 h, yielding a red powder. Anal. Calcd for **14a**, $C_{104}H_{144}N_2Na_4Nb_2O_{16}$: C, 63.86; H, 7.42; N, 1.43. Found: C, 63.45; H, 7.57; N, 1.78. ^{1}H NMR (C_5D_5N, 298 K; ppm): δ 7.34 (s, 2H, Ar H), 7.32 (s, 2H, Ar H), 7.09 (m, 2H, Ar H), 7.03 (m, 2H, Ar H), 6.95 (d, 2H, J = 2.4 Hz, Ar H), 6.88 (d, 2H, J = 2.4 Hz, Ar H), 6.74 (s, 2H, Ar H) overlapping with 6.73 (s, 2H, Ar H), 5.38 (d, 2H, J = 12.0 Hz, endo CH_2), 5.31 (d, 2H, J = 12.4 Hz, endo CH_2), 5.10 (d, 2H, J = 12.8 Hz, endo CH_2), 4.92 (d, 2H, J = 10.8 Hz, endo CH_2), 3.48 (s, 16H, DME), 3.25 (s, 24H, DME), 3.23−3.07 (m, 6H, exo CH_2), 2.77 (2H, J = 10.8 Hz, exo CH_2), 1.44 (s, 9H, Bu^t), 1.40 (s, 9H, Bu^t), 1.34 (s, 9H, Bu^t), 0.92 (s, 9H, Bu^t), 0.87 (s, 18H, Bu^t), 0.81 (s, 18H, Bu^t). The product is soluble in hydrocarbons and py, and slightly soluble in THF. Pyridine solutions of **14a** are stable to temperature, as judged from the ^{1}H NMR analysis. Crystals suitable for X-ray analysis were obtained at −24 °C from a toluene/DME solution (**14b**·$2C_4H_8O$).

Synthesis of 15a and 15b (Method A). Complex **4a** (6.04 g, 3.09 mmol) was suspended in toluene (120 mL), and the reaction mixture was stirred under a nitrogen atmosphere for 3 days, yielding a turbid brown suspension. The volume was concentrated to 50 mL, and a light brown solid was collected (4.781 g, 73%). Anal. Calcd for **15a**·$8C_7H_8$, $C_{196}H_{236}N_2Na_3Nb_3O_{14}$: C, 73.76; H, 7.45; N, 0.88. Found: C, 73.92; H, 7.66; N, 0.95. ^{1}H NMR (C_5D_5N, 298 K; ppm): δ 7.30 (s, 4H, Ar H), 7.28−7.24 (m, 16H, toluene), 7.17−7.14 (m, 24H, toluene), 7.09 (s, 16H, Ar H), 7.01 (s, 4H, Ar H), 6.05 (d, 4H, J = 12.8 Hz, endo CH_2), 5.15 (d, 8H, J = 11.6 Hz, endo CH_2), 3.64 (m, 8H, THF), 3.56 (d, 4H, J = 12.8 Hz, exo CH_2), 3.24 (d, 8H, J = 11.6 Hz, exo CH_2), 2.21 (s, 24H, toluene), 1.60 (m, 8H, THF), 1.41 (s, 18H, Bu^t), 1.13 (s, 72H, Bu^t), 0.78 (s, 18H, Bu^t). Labeled **15a** was prepared by dissolving **4a** (7.03 g, 3.60 mmol) in toluene (225 mL) and stirring the resulting solution under a $^{15}N_2$ atmosphere (98+% isotopic purity, purchased from Cambridge Isotopes Laboratory). Workup was carried out under an unlabeled N_2 atmosphere. ^{15}N NMR (C_5D_5N, 40.57 MHz, 298 K; ppm): δ 198.17. ^{15}N NMR (C_4D_8O, 40.566 MHz, 298 K; ppm): δ 197.84. ^{15}N NMR ($CDCl_3$, 40.566 MHz, 298 K; ppm): δ 213.70 (s), 198.17 (s). The product is thermally stable in deuterated pyridine and C_6D_6, as judged by the ^{1}H NMR experiments. It is soluble in THF, $CHCl_3$, and TMEDA and slightly soluble in aromatic hydrocarbons. From a room-temperature saturated $CHCl_3$/diglyme solution of the isolated powder were grown orange crystals of the diamagnetic **15b**·$9C_4H_8O$ suitable for X-ray analysis, while from a room-temperature saturated toluene/TMEDA solution it was possible to isolate white crystals of **16** suitable for X-ray analysis. The ^{1}H NMR and ^{15}N NMR spectra of **16** are very similar to those of **11b**. In a gas-volumetric experiment, **4a** (1.770 g, 0.906 mmol), dissolved in toluene (125 mL), at 288 K and 1 atm absorbed 0.6 mmol of N_2 in 24 h.

Synthesis of 15a (Method B). Complex **4a** (3.247 g, 1.66 mmol) was added to a reddish toluene (100 mL) suspension of **7a** (6.706 g, 3.38 mmol) under an argon atmosphere. The resulting reddish suspension was stirred for 2 days under an argon atmosphere, yielding a brown suspension. The volume of this suspension was reduced to 50 mL, and a yellow solid was collected (7.58 g, 71%). Anal. Calcd for **15a**·$8C_7H_8$, $C_{196}H_{236}N_2Na_3Nb_3O_{14}$: C, 73.76; H, 7.45; N, 0.88. Found: C, 74.02; H, 7.59; N, 0.97. ^{1}H NMR (C_5D_5N, 298 K; ppm): δ 7.30 (s, 4H, Ar

H), 7.28−7.24 (m, 16H, toluene), 7.17−7.14 (m, 24H, toluene), 7.09 (s, 16H, Ar H), 7.01 (s, 4H, Ar H), 6.05 (d, 4H, J = 12.8 Hz, endo CH_2), 5.15 (d, 8H, J = 11.6 Hz, endo CH_2), 3.64 (m, 8H, THF), 3.56 (d, 4H, J = 12.8 Hz, exo CH_2), 3.24 (d, 8H, J = 11.6 Hz, exo CH_2), 2.21 (s, 24H, toluene), 1.60 (m, 8H, THF), 1.41 (s, 18H, Bu^t), 1.13 (s, 72H, Bu^t), 0.78 (s, 18H, Bu^t). The isolated product has the same solubility and same color when in a solution of **15a**·$8C_7H_8$; spectroscopic analysis (NMR, IR) gave the same results. No reaction occurred upon mixing **4a** and **7a** in THF.

Synthesis of 17. The complex **15a**·$8C_7H_8$ (2.96 g, 0.93 mmol) was dissolved in $CHCl_3$ (40 mL), yielding a reddish solution. TMEDA (5 mL) was added, and the resulting solution was allowed to stand at room temperature for 24 h, after which it was concentrated to 25 mL. The yellow powder that precipitated was collected (1.03 g, 51%). Anal. Calcd for **17**·$2.5CHCl_3$, $C_{102.5}H_{138.5}Cl_{7.5}N_5NaNb_2O_8$: C, 60.25; H, 6.83; N, 3.43. Found: C, 60.03; H, 7.03; N, 3.27. ^{1}H NMR (C_5D_5N, 298 K; ppm): δ 8.53 (s, 2.5H, $CHCl_3$), 7.23 (s, 16H, Ar H), 5.41 (d, 8H, J = 11.7 Hz, endo CH_2), 3.36 (d, 8H, J = 11.7 Hz, exo CH_2), 2.38 (s, 8H, TMEDA), 2.16 (s, 24H, TMEDA), 1.16 (s, 72H, Bu^t). Attempts to isolate other reaction products failed. When labeled **17** (0.028 g, 0.017 mmol) was added to a C_5D_5N solution of **11a** (0.010 g, 0.008 mmol), ^{1}H NMR analysis showed clean formation of **15a**, while a singlet at 198.83 ppm was observed in the ^{15}N NMR spectrum. The same experiment with the same result was performed using C_4H_8O instead of C_5D_5N. Isotopically labeled **17** was prepared from labeled **15**. Workup was carried out under unlabeled N_2. ^{15}N NMR (C_5D_5N, 40.57 MHz, 298 K; ppm): δ 167.72. ^{15}N NMR ($CDCl_3$, 40.57 MHz, 298 K; ppm): δ 160.93. Crystals suitable for X-ray analysis were grown in a TMEDA/PhCl solution (**17**·$5C_6H_5Cl$).

Synthesis of 15b from 17. The complex **17**·$4CHCl_3$ (0.411 g, 0.176 mmol) was dissolved in toluene (50 mL), and then **11a** (0.178 g, 0.088 mmol) was added. The resulting yellow solution was stirred for 12 h, and ^{1}H NMR (C_5H_5N) of the crude sample showed **15** as the only product detectable in solution. The solvent was concentrated to 10 mL, the reaction mixture was stored at −24 °C for 24 h, and **15** was then collected as a yellow solid (0.250 g). ^{1}H NMR (C_5D_5N, 298 K; ppm): δ 7.30 (s, 4H, Ar H), 7.28−7.24 (m, 16H, toluene), 7.17−7.14 (m, toluene), 7.09 (s, 16H, Ar H), 7.01 (s, 4H, Ar H), 6.05 (d, 4H, J = 12.8 Hz, endo CH_2), 5.15 (d, 8H, J = 11.6 Hz, endo CH_2), 3.56 (d, 4H, J = 12.8 Hz, exo CH_2), 3.24 (d, 8H, J = 11.6 Hz, exo CH_2), 2.36 (s, TMEDA), 2.21 (s, toluene), 2.15 (s, TMEDA), 1.41 (s, 18H, Bu^t), 1.13 (s, 72H, Bu^t), 0.78 (s, 18H, Bu^t).

X-ray Crystallography of Complexes 4b, 7c, 11b, 12b, 13b, 15b, and 17. Single crystals suitable for X-ray diffraction were grown from common organic solvents (Table 1). Data for **4b**, **7c**, and **11b** were collected on a Rigaku AFC6S diffractometer using Cu Kα radiation, those for **12b** and **17** were acquired with a Kuma KM4CCD instrument, and those for **13b** and **15b** were collected on a MAR345 image plate diffractometer using Mo Kα radiation. Solutions and refinements were carried out using the programs SHELX76[13] and SHELXL93.[14] Details of the X-ray data collections and structure solutions and refinements are available.[15]

Results

(a) Four-Electron Reduction of Dinitrogen. The pathway leading to reduced niobium species bonded to the *p*-Bu^t-calix[4]arene tetraanion is displayed in Scheme 1. The synthesis of the starting material **1** was achieved by a direct reaction between $NbCl_5$ and the calix[4]arene *p*-Bu^t-calix[4]-$(OH)_4$ in toluene, leading to a quantitative yield of **1**. The proposed dinuclear structure is based on a preliminary X-ray analysis,[16] which is not included in the present account, and is supported by the ^{1}H

Table 1. Crystal Data and Experimental Details for the X-ray Diffraction Studies of **4b**, **7c**, **11b**, **12b**, **13b**, **15b**, and **17**

complex	**4b**	**7c**	**11b**	**12b**	**13b**	**15b**	**17**
empirical formula	$C_{96}H_{124}Na_2Nb_2O_{12}$·$6C_7H_8$	$C_{100}H_{116}N_2Nb_2O_8$·$2C_{12}H_{28}NaO_6$	$C_{104}H_{144}N_2Na_4Nb_2O_{16}$·$6C_6H_5Cl$	$C_{108}H_{154}N_2Na_4Nb_2O_{18}$·$5C_4H_{10}O_2$	$C_{104}H_{144}N_2Na_4Nb_2O_{17}$·$2C_4H_{10}O_2$	$C_{149}H_{192}N_3Na_3Nb_3O_{15.5}$·$9C_4H_8O$	$C_{88}H_{104}NNb_2O_8$·$C_{12}H_{32}NaN_4$·$5C_6H_5Cl$
a, Å	19.838(3)	12.950(2)	17.086(3)	15.935(2)	12.823(5)	41.535(8)	17.089(2)
b, Å	16.009(3)	12.950(2)	17.767(3)	20.285(2)	19.384(5)	27.956(6)	39.590(3)
c, Å	21.159(3)	40.164(5)	12.709(2)	22.558(2)	24.766(6)	36.219(7)	18.047(3)
α,deg	90	90	101.49(2)	70.88(2)	102.55(2)	90	90
β, deg	110.14(2)	90	104.63(1)	85.31(2)	94.22(3)	104.79(3)	93.97(2)
γ, deg	90	90	66.10(1)	79.33(2)	101.31(3)	90	90
V, Å^3	6308.9(19)	6735.6(17)	3392.3(10)	6768.6(15)	5849(3)	40662(15)	12180(3)
Z	2	2	1	2	2	8	4
fw	2254.7	2242.5	2631.4	2496.8	2152.3	3269.8	2307.8
space group	$P2_1$ (No. 4)	*P4/nnc* (No. 126)	$P\bar{1}$ (No. 2)	$P\bar{1}$ (No. 2)	$P\bar{1}$ (No. 2)	*C*2/*c* (No. 15)	*C*2/*m* (No. 12)
t, °C	−130	22	−130	22	−138	22	−130
λ, Å	1.541 78	1.541 78	1.541 78	0.710 69	0.710 69	0.710 69	0.710 69
ρ_{calc}, g cm^{-3}	1.187	1.106	1.288	1.225	1.222	1.068	1.258
μ, cm^{-1}	20.12	19.29	31.26	2.38	2.62	2.019	3.48
transmission coeff	0.517−1.000	0.438−1.000	0.739−1.000	0.671−1.000	0.685−1.000	0.979−1.000	0.978−1.000
R1[a]	0.056 [0.058][b]	0.075	0.063	0.097	0.055	0.096	0.094
wR2	0.167 [0.169][b]	0.230	0.186	0.243	0.138	0.277	0.218
GOF	1.071	0.960	1.037	1.079	1.059	1.123	1.180
N_o[c]	6621	869	5043	14 619	11 780	9860	10 815
N_t[d]	10 197	2076	9227	25 586	17 140	23 590	16 322
N_r[e]	9380	2020	8027	14 619	11 780	12 998	10 815
no. of variables	1281	170	704	1438	1260	1656	654

[a] Calculated on the observed reflections. [b] Values in brackets refer to the "inverted" structure. [c] Total number of the independent reflections having $I > 2\sigma(I)$ for **4b**, **7c**, **11b**, **12b**, **13b**, and **15b** and $I > 3\sigma(I)$ for **17**. [d] Number of independent reflections. [e] Number of reflections used in the refinement having $I > 0$ for **4b**, **7c**, and **11b**, $I > \sigma(I)$ for **15b**, $I > 2\sigma(I)$ for **12b** and **13b**, and $I > 3\sigma(I)$ for **17**.

(13) Sheldrick, G. M. *SHELX76*: *Program for crystal structure determination*. University of Cambridge: Cambridge, England, 1976.

(14) Sheldrick, G. M. *SHELXL93*: *Program for crystal structure refinement*; University of Göttingen: Göttingen, Germany, 1993.

(15) See paragraph at end of paper regarding Supporting Information.

(16) Zanotti-Gerosa, A.; Solari, E.; Giannini, L.; Floriani, C.; Re, N.; Chiesi-Villa, A.; Rizzoli, C. *Chem. Commun.* **1997**, 183. Also: unpublished results.

Scheme 1

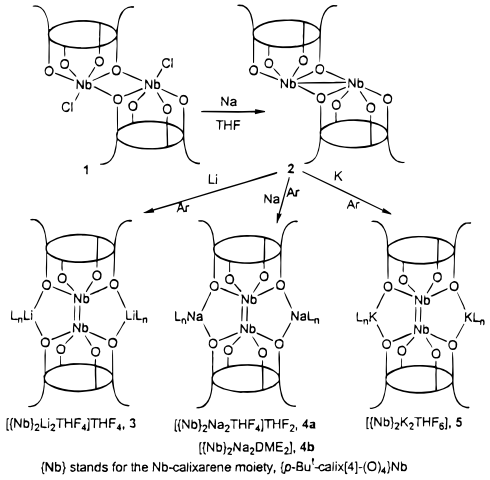

NMR spectrum, which indicates C_i symmetry for the calix[4]-arene fragment and exhibits two pairs of doublets for the bridging methylene. The elliptical deformation of the usual cone conformation of the calix fragment is the consequence of binding to a hexacoordinated metal.[16]

The reduction of **1** was carried out in a stepwise manner. The first step, performed by reacting **1** with Na metal in the presence of a catalytic amount of naphthalene, led to the diamagnetic Nb(IV)−Nb(IV) dimer containing an Nb−Nb single bond [2.759(1) Å].[17] The reduction of **2** was carried out under an argon atmosphere. Reduction with Li, Na, and K, performed as detailed in the Experimental Section, gave very similar compounds, shown as **3**−**5** in Scheme 1 (for the sake of clarity, in all schemes, where appropriate, the number of a compound is given with a letter identifying the solvation of the alkali metal cation). All of these compounds are diamagnetic. The ^{1}H NMR spectra were recorded for only **3** and **4**, complex **5** being insufficiently stable. The spectra of **3** in both TDF and toluene-d_8 show an apparent D_{2h} symmetry with a single pair of doublets for the bridging methylenes and two singlets for the Bu^t substituents. The same apparent symmetry is found in the ^{1}H NMR spectrum of **4a** in toluene-d_8 recorded at low temperature (−40 °C), while the ^{1}H NMR spectrum of **4a** in THF displays a 4-fold symmetry, with a single pair of doublets for the methylenes and a singlet for the four Bu^t substituents. On the basis of the structure of **4b** (see below), we assume that, in compounds **3**−**5**, the alkali metal cations bridge the two calix-[4]arene ligands. The labeling scheme adopted for the calixarene−Nb moiety for all complexes is given in Chart 1. Selected bond distances and angles are listed in Table 2 for complexes **4b**, **7c**, **11b**, and **12b** and in Table 3 for complexes **13b**, **15b**, and **17**. In Table 4 is given a comparison of relevant conformational parameters within the [Nb(calix[4]arene)] units. Complex **4b** displays a dimeric structure (Figure 1) containing an Nb═Nb double bond [2.659(1) Å][18] (structural parameters in Table 2 are related to the A unit of the dimer). The Nb−Nb vector forms an angle of 0.9(2)° [1.3(2)°] with the normal to the O_4 plane. The coordination environment of the Nb═Nb unit can be described as a distorted tetragonal prism, the niobium atoms lying roughly at the center of the two opposite O_4 faces which form a dihedral angle of 0.8(2)°, with the metal being displaced 0.372(1) Å from the O_4 mean plane (Table 4). Nb−O(1) and Nb−O(4) are much longer than the Nb(1)−O(1) and Nb(1)−O(3) bond distances (Table 2). The two sodium cations are located across two calix units, and they complete their tetrahedral coordination with a DME molecule.

Chart 1. Labeling Scheme Adopted for the Calixarene Macrocycle.

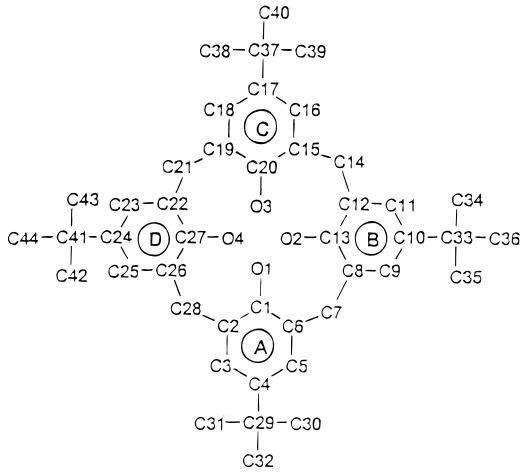

The nature of the alkali metal cation along with its solvation, derived from either the reaction or crystallization solvent, affects both the stability of the dimeric structure and its reactivity with substrates (see below) and in particular with N_2 (Scheme 2). In the case of the lithium derivative **3**, a very slow reaction with N_2, leading to **6a**,[19] was observed in THF, while no reaction was observed in toluene. The formation of the same compound, though with a different solvation sphere around the lithium, was achieved by replacing sodium with lithium in the reaction of **7a** with LiCl (see Scheme 2). Complex **7a** was obtained equally well by exposing a THF solution of **4a** to an N_2 atmosphere or by reducing **2** under argon in THF followed by exposure to N_2. The reactions in THF gave the solvated form **7a**, which was converted to **7b** during recrystallization from DME. Other solvated forms, namely **7c** and **7d**, were obtained in the presence of diglyme and 18-crown-6 ether, respectively (see the Experimental Section). The Nb−K couple, complex **5**, behaved very similarly to what was observed in the case of the Nb−Na derivative **4** and under N_2 led to the formation of **8a** and **8b** in THF and DME, respectively. Due to some instability of **5**, the reaction with N_2 was preferentially carried out by reducing **2** with K under a nitrogen atmosphere. The dinitrogen complexes **6**−**8** are diamagnetic, the ^{1}H NMR spectra agree with a C_{4v} symmetry for the calix[4]arene fragment, and we assume that all of them contain the dianion present in **7c**, as shown in Figure 2.

The dimeric anion has a crystallographically imposed C_4 symmetry, the 4-fold axis running through the niobium atoms and the nitrogen atoms. Coordination around the one independent niobium atom is square pyramidal involving the four oxygen atoms at the base and a nitrogen atom at the apex. The metal is displaced 0.445(1) Å from the planar O_4 core toward the N(1) atom (Table 4). The Nb−N axis is strictly perpendicular to the O_4 core from symmetry requirements. As expected for five-coordinated metallacalix[4]arenes, the calix moiety assumes a regular cone conformation. The Nb−N [1.747(12) Å][20] and N−N [1.390(17) Å][3] distances and the linearity of the Nb−N−N−Nb skeleton support the four-electron reduction of N_2

(17) C. Floriani et al., unpublished results.

(18) Cotton, F. A.; Walton, R. A. *Multiple Bonds Between Metal Atoms*, 2nd ed.; Oxford University Press: New York, 1993.

(19) A few niobium−dinitrogen compounds have been reported. See ref 3e and the following references: (a) Dilworth, J. R.; Henderson, R. A.; Hills, A.; Hughes, D. L.; Macdonald, C.; Stephens, A. N.; Walton, D. R. M. *J. Chem. Soc., Dalton Trans.* **1990**, 1077. (b) Berno, P.; Gambarotta, S. *Organometallics* **1995**, *14*, 2159.

Table 2. Selected Bond Distances (Å) and Angles (deg) for **4b**, **7c**, **11b**, and **12b**

Complex **4b**

Nb(1)A−Nb(1)B	2.659(1)	Nb(1)−O(2)	2.097(6)	Nb(1)−O(4)	2.085(9)
Nb(1)−O(1)	1.903(8)	Nb(1)−O(3)	1.947(9)		

Complex **7c**[a]

Nb(1)−O(1)	1.994(8)	Nb(1)−N(1)	1.747(12)	N(1)−N(1)″	1.390(17)
		Nb(1)−N(1)−N(1)″	180.0(−)		

Complex **11b**[b]

Nb(1)−O(1)	2.113(6)	Nb(1)−O(2)	2.074(6)	Nb(1)−O(3)	2.119(5)
Nb(1)−O(4)	2.083(6)	Nb(1)−N(1)	1.910(6)	Nb(1)−N(1)′	1.909(7)
Na(1)−N(1)	2.438(1)				
N(1)−Nb(1)−N(1)′	85.7(3)	Nb(1)−N(1)−Nb(1)′	94.3(3)		

Complex **12b**[c]

	A	B		A	B
Nb(1)A−Nb(1)B	2.635(1)		Nb(1)−O(4)	2.175(4)	2.081(4)
Nb(1)A−O(1)B	2.097(5)		Nb(1) − N(1)	2.107(9)	2.078(6)
Nb(1)−O(1)	2.136(6)	2.078(7)	Nb(1)−N(2)	2.133(9)	2.079(6)
Nb(1)−O(2)	2.180(4)	2.099(5)	N(1)−N(2)	1.403(8)	
Nb(1)−O(3)	2.053(5)	2.142(6)	N(1)−Nb(1)−N(2)	38.6(3)	39.4(3)

[a] Double prime = x, 0.5 − y, 0.5 − z. [b] Single prime = $-x$, $-y$, $-z$. [c] A and B refer to the two halves of the dimer.

Table 3. Selected Bond Distances (Å) and Angles (deg) for **13b**, **15b**, and **17**

Complex **13b**[a]

	A	B		A	B
Nb(1)−O(1)	2.085(3)	2.071(3)	Nb(1)A−O(7)	1.961(3)	1.909(4)
Nb(1)−O(2)	2.151(4)	2.162(3)	Nb(1)−N(1)	2.056(5)	2.054(4)
Nb(1)−O(3)	1.956(4)	2.021(4)	Nb(1)−N(2)	2.053(5)	2.067(4)
Nb(1)−O(4)	2.117(4)	2.140(4)	N(1)−N(2)	1.424(5)	
N(1)−Nb(1)−N(2)	40.6(2)	40.4(2)	N(1)A−O(7)−Nb(1)B	38.6(3)	39.4(3)

Complex **15b**[b]

	A	B	C
Nb(1)−O(1)	1.942(8)	2.027(11)	2.019(7)
Nb(1)−O(2)	2.025(9)	1.983(7)	2.037(9)
Nb(1)−O(3)	1.984(8)	1.950(6)	1.932(6)
Nb(1)−O(4)	1.911(12)	1.951(8)	1.952(8)
Nb(1)−N(1)	2.008(10)		1.782(10)
Nb(1)−N(2)	1.980(10)	1.770(12)	
N(1)−Nb(1)−N(2)	89.3(4)	Nb(1)A−N(1)−Nb(1)C	168.7(6)
Nb(1)A−N(2)−Nb(1)B	159.3(6)		

Complex **17**[c]

Nb(1)−O(1)	1.924(4)	Nb(1)−O(2)	1.948(3)	Nb(1)−O(3)	1.946(4)
Nb(1)−O(4)	1.952(4)	Nb(1)−N(1)	1.854(2)		
		Nb(1)−N(1)−Nb(1)′	145.2(1)		

[a] A and B refer to the two units of the dimer. [b] A−C refer to the three units of the trimer. [c] A prime denotes the transformation of x, 1 − y, z.

and the presence of an Nb≡N pseudo triple bond. The resonance Raman spectrum of **7a** in the solid state shows an N−N stretching frequency at 1372 cm^{-1}, in agreement with a significant elongation of the dinitrogen bond and a decrease of the N−N bond order from 3 in N_2[21] to a value between 1 and 2.[4,22] The $^{15}N-^{15}N$ stretching frequency is, as expected, shifted down to 1328 cm^{-1}.[4,22] The Nb−O bond distances [1.994(8) Å] are relatively long because of the limited oxygen-to-metal π bonding, which is hindered by the presence of the Nb≡N triple bond. Niobium(V) is expected to be a rather strong Lewis acid in complexes **7a**−**d**, even though the only available coordination site is inside the calix cavity. Bu^{t}NC, which has a suitable shape for entering the calix cavity,[23] converted **7a** into **9a** (see Scheme 3). The significant increase in the C−N stretching frequency up to 2206 cm^{-1} reflects the high acidity of the metal center. The binding to the metal of a strong σ base affects the structural parameters and, as a consequence, the chemical properties (see below) of the Nb≡N−N≡Nb moiety. Although the X-ray structure of **9b** is not of high quality,[24] some structural parameters are particularly significant, namely the elongation of the Nb−N bond distance from 1.747(12) Å in **7c** to 1.810(8) Å in **9** and the shortening of the N−N bond from 1.390(17) Å in **7c** to 1.303(11) Å in **9**. These structural parameters are similar to those of [{Nb(S_2CNEt_2)$_3$}$_2$(μ-N_2)].[19a]

(20) (a) Green, M. L. H.; James, J. T.; Saunders: J. F.; Souter, J. *J. Chem. Soc., Dalton Trans.* **1997**, 1281. (b) Nugent, W. A.; Mayer, J. M. *Metal-Ligand Multiple Bonds*; Wiley: New York, 1988; Chapter 5, p 179. (c) Cotton, F. A.; Duraj, S. A.; Roth, W. J. *J. Am. Chem. Soc.* **1984**, *106*, 4749. (d) Tan, L. S.; Goeden, G. V.; Haymore, B. L. *Inorg. Chem.* **1983**, *22*, 1744. (e) Lockwood, M. A.; Fanwick, P. E.; Eisenstein, O.; Rothwell, I. P. *J. Am. Chem. Soc.* **1996**, *118*, 2762.

(21) Rasetti, F. *Proc. Natl. Acad. Sci. U.S.A.* **1929**, *15*, 234.

(22) Cohen, J. D.; Mylvaganam, M.; Fryzuk, M. D.; Loehr, T. M. *J. Am. Chem. Soc.* **1994**, *116*, 9529.

(23) For example: (a) Castellano, B.; Solari, E.; Floriani, C.; Scopelliti, R. *Inorg. Chem.* **1999**, *38*, 3406. (b) Giannini, L.; Solari, E.; Floriani, C.; Re, N.; Chiesi-Villa, A.; Rizzoli, C. *Inorg. Chem.* **1999**, *38*, 1439.

Table 4. Comparison of Relevant Conformational Parameters within the Calixarenes for **4b**, **7c**, **11b**, **12b**, **13b**, **15b**, and **17**

	4b				**12b**		**13b**		**15b**			
	mol A	mol B	**7c**	**11b**	mol A	mol B	mol A	mol B	mol A	mol B	mol C	**17**
					(a) Distances (Å) of Atoms from the O_4 Mean Plane							
O(1)	−0.110(8)	−0.128(8)	0(−)			0.085(5)				−0.009(12)	−0.023(7)	−0.026(4)
O(2)	0.101(8)	0.139(8)	0(−)			−0.101(6)				0.004(8)	0.022(7)	0.026(4)
O(3)	−0.119(9)	−0.141(8)	0(−)			0.083(5)				−0.004(8)	−0.023(7)	−0.026(4)
O(4)	0.129(9)	0.128(8)	0(−)			−0.085(5)				0.005(9)	0.024(7)	0.026(4)
Nb	0.372(1)	0.403(1)	0.445(1)			0.329(2)				0.426(2)	0.413(2)	0.500(1)
					(b) Dihedral Angles (deg) between Planar Moieties[a]							
E∧A	129.5(3)	130.1(3)	123.9(−)	167.1(2)	163.7(2)	121.7(2)	167.2(2)	162.3(2)	159.8(4)	121.2(3)	124.5(3)	132.3(1)
E∧B	111.6(3)	117.2(3)	123.9(−)	114.5(2)	113.0(2)	116.8(2)	112.0(1)	117.0(1)	119.2(4)	119.7(4)	102.8(3)	117.0(1)
E∧C	138.5(3)	135.3(3)	123.9(−)	170.1(2)	158.2(2)	116.9(2)	146.9(1)	158.0(1)	162.4(4)	130.3(4)	128.9(4)	129.2(1)
E∧D	114.6(3)	111.0(3)	123.9(−)	110.4(2)	112.1(2)	121.5(2)	117.4(1)	110.4(2)	119.6(3)	120.4(3)	125.4(4)	120.5(1)
A∧C	92.0(4)	94.5(4)	112.3(3)	157.3(2)	140.9(3)	121.4(3)	134.2(2)	140.2(2)	142.2(4)	108.5(4)	106.6(4)	98.5(2)
B∧D	133.9(4)	131.8(3)	112.3(3)	135.1(3)	134.8(2)	121.6(3)	130.6(2)	132.6(2)	121.2(5)	119.9(4)	121.8(5)	122.5(2)
					(c) Contact Distances (Å) between Para Carbon Atoms of Opposite Aromatic Rings [b]							
C(4)···C(17)	9.2557(18)	9.265(18)	8.413(20)	10.753(16)	10.523(15)	8.165(18)	10.296(13)	10.501(14)	10.45(4)	8.53(2)	8.67(2)	9.018(8)
C(10)···C(24)	7.303(15)	7.431(15)	8.413(20)	7.229(13)	7.263(11)	7.989(12)	7.470(8)	7.361(8)	7.86(2)	8.018(20)	7.97(2)	7.768(9)

[a] E (reference plane) refers to the least-squares mean plane defined by the C(7), C(14), C(21), and C(28) bridging methylenic carbons. A−D are defined in Chart 1. [b] For complex **7c**, C(10), C(17), and C(24) should be read C(4)′, C(4)″, and C(4)*, respectively. The prime, double prime, and star, respectively, denote the following transformations: $0.5 - y, x, z$; $0.5 - x, 0.5 - y, z$; $y, 0.5 - x, z$.

Figure 1. SCHAKAL view of complex **4b**. Disorder affecting the butyl groups and one toluene guest molecule has been omitted for clarity.

Scheme 2

The hydrazido group present in **7a** can be transferred to an organic carbonyl by taking advantage of the oxophilicity of niobium. The reaction of **7a** with benzaldehyde led to the isolation of the oxoniobium(V)−calix[4]arene complex **10**[25] and the dibenzylideneazine. This kind of chemical proof was reported several years ago by Schrock.[3c,f,g]

(24) Crystal data for **9b**: $C_{104}H_{136}N_4NaNb_2O_{11}\cdot C_{12}H_{26}NaO_6$, $M = 2118.4$, orthorhombic, space group *Pmma*, $a = 25.509(5)$ Å, $b = 39.248(7)$ Å, $c = 12.791(2)$ Å, $V = 12896(4)$ Å^3, $Z = 4$, $D_{calcd} = 1.099$ g/cm^3, $F(000) = 4512$, λ(Mo Kα) = 0.710 69 Å, μ(Mo Kα) = 2.31 cm^{-1}, crystal dimensions 0.21 × 0.25 × 0.35 mm. For 5311 unique observed reflections [$I > 2\sigma(I)$] collected at 130 K on a MAR345 image plate diffractometer ($5 > 2\theta > 49°$), R1 = 0.126 (wR2 = 0.326).

(25) Caselli, A.; Solari, E.; Scopelliti, R.; Floriani, C. *J. Am. Chem. Soc.* **1999**, *121*, 8296.

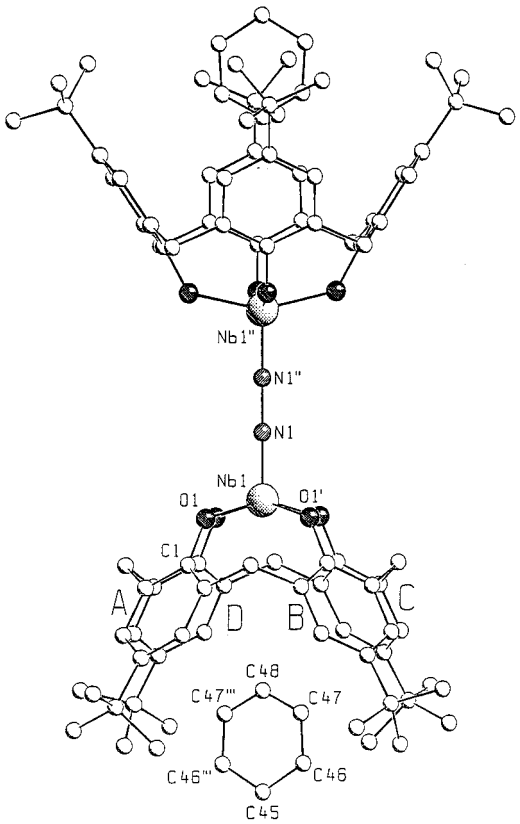

Figure 2. SCHAKAL view of the anion in complex **7c**. The prime, double primes, and triple primes denote the transformations 0.5-*y*, *x*, *z*; *x*, 0.5-*y*, 0.5-*z*; and 0.5-*x*, 0.5-*y*, *z*, respectively. Disorder involving the guest benzene molecule has been omitted for clarity.

Scheme 3

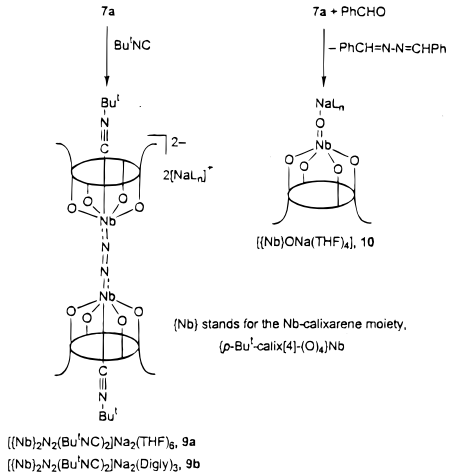

(b) Two-Electron Reduction of a Metallahydrazone: Formation of Nitrides. Two-electron reduction of **7a** using sodium metal led to the cleavage of the residual N−N bond and to the formation of the bis(μ-nitrido) species **11a**. The reaction was carried out in THF, and white crystals of **11a** were obtained from a black solution (Scheme 4). Also, the reaction was performed under both Ar and N_2 atmospheres with the same results. ^{1}H NMR analysis of the black solution showed the presence of lower symmetry diamagnetic compounds, **12** being the major product under other solvent conditions (see below).

The X-ray structure of **11b**, obtained upon recrystallization of **11a** from DME, is displayed in Figure 3 and shows the complete cleavage of the N−N bonds and the formation of a

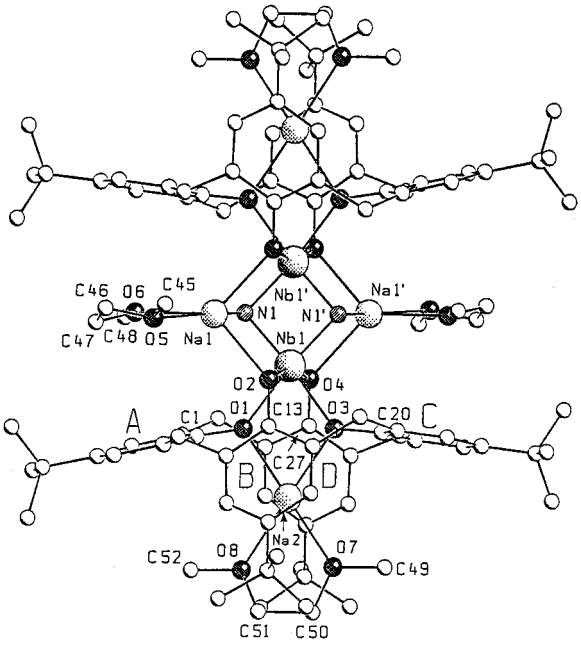

Figure 3. SCHAKAL view of complex **11b**. A prime denotes the transformation $-x$, $-y$, $-z$.

Scheme 4

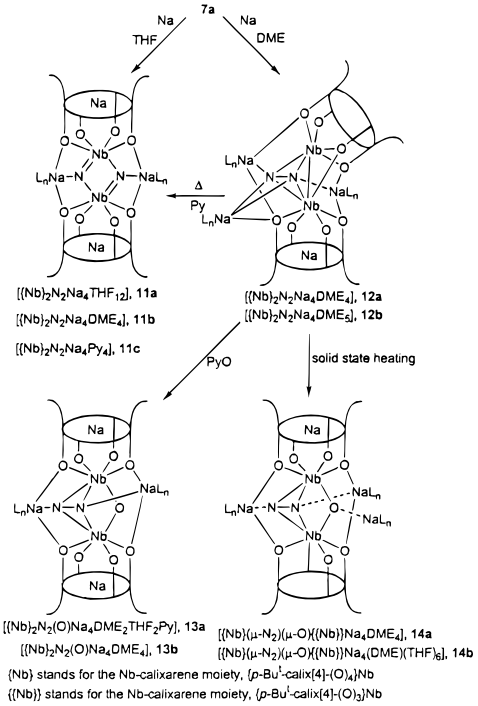

nitrido species.[4,20b,26] A few molecular Nb−nitrido species have thus far been identified, though they were prepared by using completely different synthetic routes.[27] The dimer has a crystallographically imposed C_i symmetry, the inversion center lying at the center of the Nb_2N_2 inner core, which is planar for reasons of symmetry. The Nb···Nb and N···N separations are 2.800(1) and 2.597(8) Å, respectively. Coordination around each inde-

(26) (a) *The Chemistry of Transition Metal Carbides and Nitrides*; Oyama, T., Ed.; Blackie: Glasgow, U.K., 1996. (b) Brese, N. R.; O'Keefe, M. *Struct. and Bonding* **1992**, *79*, 307. (c) Peters, J. C.; Johnson, A. R.; Odom, A. L.; Wanandi, P. W.; Davis, W. M.; Cummins, C. C. *J. Am. Chem. Soc.* **1996**, *118*, 10175. (d) Laplaza, C. E.; Johnson, A. R.; Cummins, C. C. *J. Am. Chem. Soc.* **1996**, *118*, 709. (e) Laplaza, C. E.; Odom, A. L.; Davis, W. M.; Cummins, C. C.; Protasiewicz, J. D. *J. Am. Chem. Soc.* **1995**, *117*, 4999.

pendent niobium atom is octahedral, with the O(1), O(3), N(1), and N(1)′ atoms defining the best equatorial plane and the O(2) and O(4) atoms filling the axial sites. The metal is displaced 0.011(1) Å from the equatorial plane toward the O(4) atom. The six-coordination of the metal removes the planarity of the O_4 core. As a consequence, the calixarene ligand assumes a flattened-cone conformation with the opposing A and C rings pushed outward and the opposing B and D rings pushed inward relative to the cavity of the macrocycle, as indicated by the dihedral angles they form with the "reference" plane listed in Table 4. The sodium cation Na(1) binds to N(1), O(2), and O(4)′. Its coordination is distorted trigonal bipyramidal, completed by two oxygen atoms from a DME molecule. The sodium cation Na(2) is accommodated inside the cavity of calixarene, interacting with the opposite O(1) and O(3) oxygen atoms. Coordination is completed by two oxygen atoms from a DME molecule in a nearly planar arrangement from which the cation is displaced by 0.055(4) Å. The Nb−N distances [Nb−N_{av} = 1.910(8) Å] support the bonding sequence shown in Scheme 4. The ^{1}H NMR spectrum of complex **11a**, with a single pair of doublets for the bridging methylenes and a singlet for the Bu^t substituents, suggests a 4-fold symmetry, which is in disagreement with the pseudo-2-fold symmetry of the solid-state structure. The ^{15}N NMR spectrum of **11a** showed a singlet for the resonance of the nitrido species at 269.4 ppm (193 K),[10,28] regardless of the solvent used (THF, py).

When the reduction of **7a** using Na metal was carried out in DME instead of THF, the reaction led only to a small amount of **11b**, while the majority of the reduced species remained in solution (see the Experimental Section). The addition of pentane to the residue obtained after evaporation of the DME led to the formation of green crystals of **12a** in a significant amount (∼50%) (Scheme 4). The genesis of **12a** can be understood by assuming that the two-electron reduction did not affect the N−N bond but rather caused the reduction of Nb(V) to Nb(IV) with consequent Nb−Nb bond formation (Scheme 4). This metal−metal formation caused an overall distortion of the dimeric unit, thus forcing the dinitrogen to rearrange its bonding arrangement from a terminal η^1:η^1 mode to a bridging μ-η^2:η^2 mode. While most dinuclear dinitrogen complexes contain a bridging end-on N_2,[1] the side-on bonding mode is no longer so rare.[2f,3j,22,29]

A simplified view of the dianion present in complex **12b**, a slightly different solvated form of **12a**, is given in Figure 4. The N−N axis is perpendicular to the Nb−Nb bond, the dihedral angle between the N−N and Nb−Nb vectors being 89.2(3)°. The N_2 fragment resides inside a cluster of metal ions, being μ-η^2:η^2 bonded to the two niobium ions, η^1 bonded to Na(2) and Na(4), and η^2 bonded to Na(3) (omitted shown in Figure 4 for the sake of clarity, but drawn in Scheme 4). The sodium cations complete their coordination spheres using oxygen atoms from both calix units and the DME molecules. The structural parameters in Table 4 confirm the presence of Nb−Nb [2.635(1) Å][18] and N−N [1.403(8) Å] single bonds.[3] The two Nb−calix units, which are different in shape and geometry, will be hereafter referred to as units A and B. For both the Nb−O and

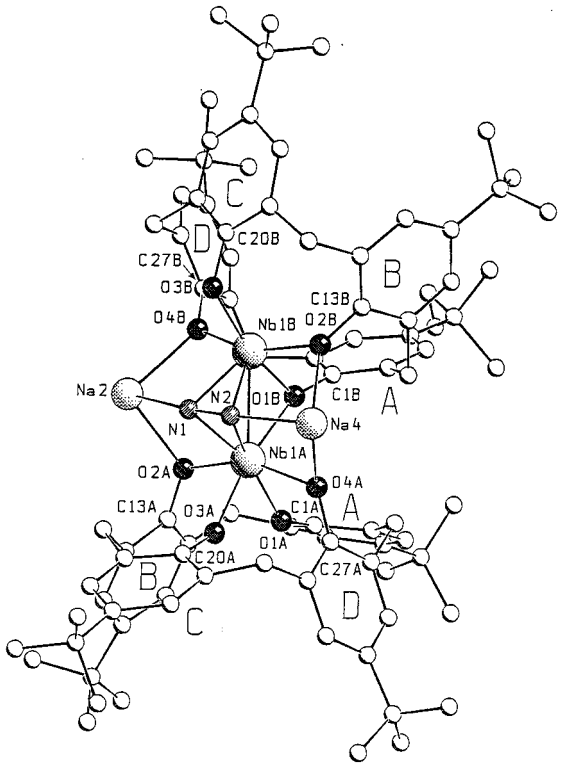

Figure 4. Simplified SCHAKAL view of complex **12b**. Na(3) bonded to N(2), the sodium cation inside the cavity, DME molecules, and disorder have been omitted for clarity.

Nb−N bond distances, the values observed in unit A (mean values 2.14(24) and 2.120(13) Å, respectively) are longer than those in unit B (mean values 2.097(13) and 2.078(5) Å, respectively), as a consequence of the higher coordination number of the metal and the difference in the calix[4]arene conformations. The Na−N distances involving the terminally bonded Na(2) and Na(4) cations (mean value 2.33(4) Å) are a little, but significantly, shorter than the distances related to the bridging Na(3) [mean value 2.47(13) Å].

Complex **12a** is not thermally very stable, and it undergoes the transformation into **11** at a temperature that depends on the solvent used, the best being pyridine. When complex **12a** was heated in pyridine at 90 °C, **11c** was formed as a unique product (Scheme 4). The thermal rearrangement of **12a** to **11c** occurs with cleavage of the Nb−Nb and the N−N bonds, as a result of the two-electron transfer from the metal−metal to the N−N bond. The reduced form **12a** can, however, undergo a two-electron oxidation using the pair of electrons stored in the metal−metal bond, without affecting the N_2 bonding mode and its reduction degree. The reaction of **12a** with O_2 or, better, with pyO led to the insertion of an oxygen atom between the two Nb ions, with dinitrogen remaining μ-η^2:η^2 bonded across the two niobium ions (see complexes **13a** and **13b** in Scheme 4). The structure of **13b**, displayed in Figure 5, shows the arrangement of both the oxo and the N_2 bridging ligands. The N−N bond is perpendicular to the Nb···Nb vector [dihedral angle 89.5(2)°]. The Na(2) and Na(3) ions interact with N(1) and N(2), respectively, at distances close to those in **12b** [mean value 2.360(9) Å]. Coordination around each sodium cation is completed by DME oxygens. The bonding picture (Scheme 4) proposed for **13b** is supported by the values for the N−N single bond [1.424(5) Å],[3] the Nb···Nb separation [2.876(9) Å], the Nb−O(oxo) bond distances [1.961(3) and 1.909(4) Å], the Nb(1)A−O(7)−Nb(1)B angle [96.0(1)°], and the Nb−N single-

(27) (a) Horner, M.; Frank, K. B.; Strähle, J. *Z. Naturforsch.* **1986**, *41B*, 423. (b) Dehnicke, K.; Strähle, J. *Angew. Chem., Int. Ed. Engl.* **1981**, *20*, 413.

(28) (a) Zanetti, N. C.; Schrock, R. R.; Davis, W. M.; Wanninger, K.; Seidel, S. W.; O'Donoghue, M. B. *J. Am. Chem. Soc.* **1997**, *119*, 11037. (b) Laplaza, C. E.; Cummins, C. C. *Science* **1995**, *268*, 861.

(29) (a) Fryzuk, M. D.; Johnson, S. A.; Rettig, S. J. *J. Am. Chem. Soc.* **1998**, *120*, 11024. (b) Evans, W. J.; Ulibarri, T. A.; Ziller, J. W. *J. Am. Chem. Soc.* **1988**, *110*, 6877. (c) Cohen, J. D.; Fryzuk, M. D.; Loehr, T. M.; Mylvaganam, M.; Rettig, S. J. *Inorg. Chem.* **1998**, *37*, 112. (d) Roussel, P.; Scott, P. *J. Am. Chem. Soc.* **1998**, *120*, 1070. (e) Jeffery, J.; Lappert, M. F.; Riley, P. I. *J. Organomet. Chem.* **1979**, *181*, 25.

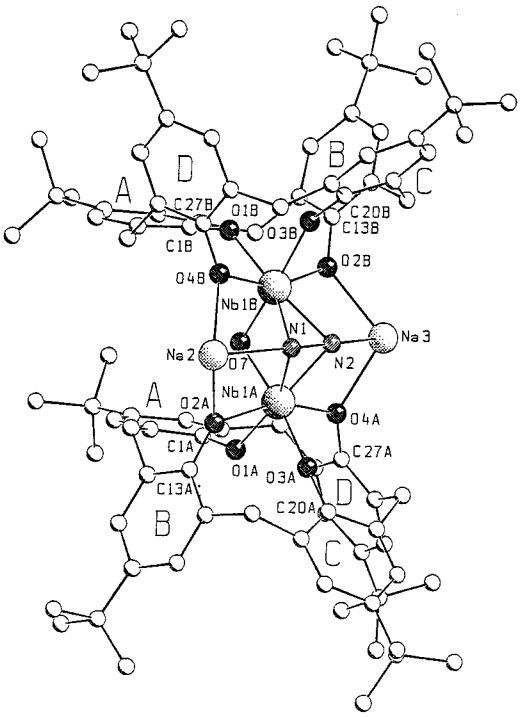

Figure 5. Simplified SCHAKAL view of complex **13b**. Sodium cations inside the cavity, DME molecules, and disorder have been omitted for clarity.

bond distances, averaging to 2.058(7) Å. The coordination around niobium is similar to that observed in unit A of complex **12b**. The two remaining Na cations reside in the calix[4]arene cavity.

Complex **13** undergoes no thermal rearrangement because the two electrons stored in the Nb−Nb bond in **12** are no longer available. The availability of the two electrons stored in the Nb−Nb bond in **12** for the reductive cleavage of covalent bonds other than the N−N bond has been illustrated by heating complex **12a** in the solid state. The compound formed is displayed in Scheme 4 as complex **14a**. The thermal rearrangement can be described as the result of the a two-electron transfer from the Nb−Nb bond to a C−O bond of one of the phenoxo groups.[30] This process causes the cleavage of the C−O bond, the generation of a μ-oxo species, and the formation of an Nb−C bond with one of the phenyl groups of the calix moiety. The proposed structure is supported by an X-ray analysis,[31] even though carried out on medium-quality crystals of **14b** obtained from crystallization of **14a** in THF. This determination provided us with useful information regarding the atom connectivity and the main structural parameters [Nb−N = 2.047(12) Å; Nb−O(oxo)$_{av}$ = 1.990(8) Å; N−N = 1.35(2) Å; Nb(1)−C = 2.454(18) Å].

(c) Direct Formation of Nitrides from Dinitrogen in a Nonstepwise Manner. The reaction of **4a** with dinitrogen is strongly dependent on the nature of the solvent. In polar solvents, namely ethers (THF, DME), the reaction led to the formation of the dinitrogen complexes **7**. When the same reaction was carried out in toluene, a nitrido complex, labeled

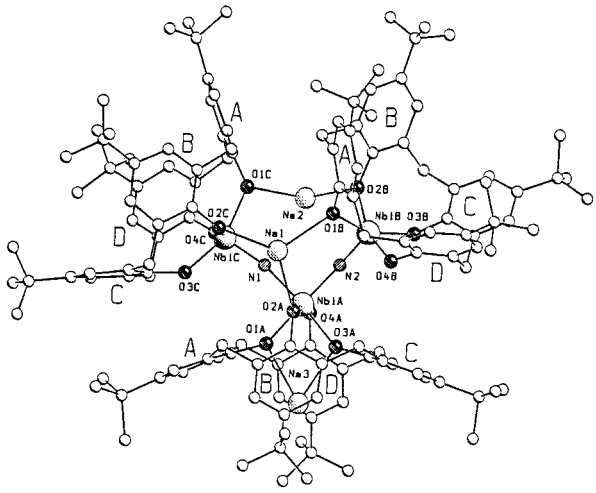

Figure 6. Simplified SCHAKAL view of complex **15b**. The solvent molecules bonded to the Na cations and disorder have been omitted for clarity.

Scheme 5

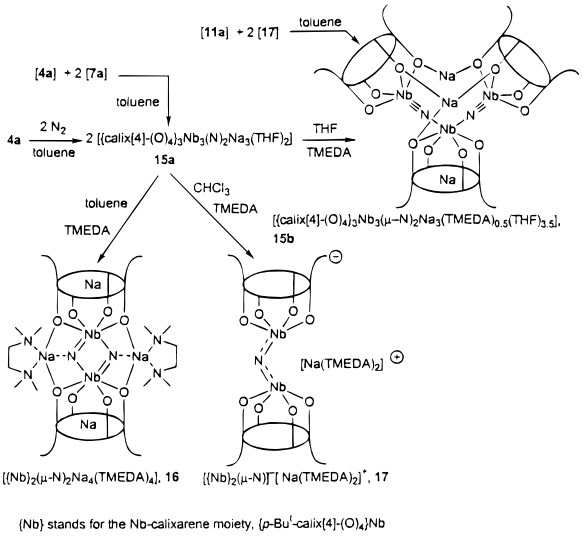

as **15a** in Scheme 5, was obtained. The gas-volumetric absorption of N_2, as well as its hydrolysis, confirmed the 3:2 Nb:N molar ratio. Complex **15a** was obtained equally well from the reaction of **4a** and **7a** in a 1:2 molar ratio carried out in toluene, while no reaction occurred upon mixing the two components in THF. The ^{1}H NMR spectrum of **15a**, in either THF or py, shows the presence of calix[4]arene moieties with 2- and 4-fold symmetries in a 1:2 ratio, while a singlet at 198.2 ppm is found in the ^{15}N NMR spectrum. The ^{1}H NMR spectrum of **15a** in $CDCl_3$ is quite complex, while the ^{15}N NMR spectrum indicates the presence of two singlets at 213.7 and 176.8 ppm. Complex **15a**, when recrystallized from THF in the presence of small amounts of TMEDA, gave the solvated form **15b**, shown in Figure 6.

The structure of **15b** consists of trimeric complex molecules and THF and TMEDA solvent molecules in a stoichiometric trimer:THF:TMEDA molar ratio of 1:12.5:0.5. The Na(1) and Na(2) cations interact with oxygen atoms of three and two calixarene ligands, respectively. A third Na cation is accommodated by the cavity of the calixarene A unit. Coordination around niobium in unit A is octahedral, the best equatorial plane being defined by the N(1), N(2), O(1)A, and O(3)A atoms (the deviations from the planarity range from −0.020(11) to +0.020(11) Å). The metal is displaced 0.084(2) Å from the equatorial

(30) Baumann, R.; Stumpf, R.; Davis, W. M.; Liang, L.-C.; Schrock, R. R. *J. Am. Chem. Soc.* **1999**, *121*, 7822 and references therein.

(31) Crystal data for **14b**·2THF: $C_{116}H_{162}N_2Na_4Nb_2O_{16}$·$2C_4H_8O$, M = 2262.5, triclinic, space group $P\bar{1}$, a = 15.959(2) Å, b = 16.712(2) Å, c = 24.815(3) Å, α = 89.42(1)°, β = 84.70(1)°, γ = 71.88(1)°, V = 6262(14) Å^3, Z = 2, D_{calcd} = 1.200 g/cm^3, $F(000)$ = 2412, λ(Mo Kα) = 0.710 69 Å, μ(Mo Kα) = 2.46 cm^{-1}, crystal dimensions 0.17 × 0.20 × 0.25 mm. For 9044 unique observed reflections [$I > 2\sigma(I)$] collected at 130 K on a Kuma KM4CCD diffractometer ($5 > 2\theta > 59°$), R1 = 0.153 (wR2 = 0.301).

mean plane toward O(4)A. The coordination polyhedron around the metal in both unit B and unit C is square pyramidal. The Nb−N vectors in units B and C form dihedral angles of 3.4(4) and 3.2(4)°, respectively, with the normals to the mean planes through the O_4 systems. The Nb(1)A−N distances [2.008(10) and 1.980(10) Å] are in the range expected for a single bond, and the Nb(1)B−N(2) [1.770(12) Å] and Nb(1)C−N(1) distances [1.782(10) Å] are in agreement with the presence of triple bonds. The nearly planar Nb−N−Nb skeletons [Nb(1)A−N(1)−Nb(1)C = 168.7(6) Å and Nb(1)A−N(2)−Nb(1)B = 159.3(6) Å] support the sp hybridization of the bridging nitrides. The Na···N contacts are not very significant, the shortest one being Na(1)···N(1) = 2.810(14) Å and the other one being greater than 3.0 Å. Calixarene unit A shows an elliptical conformation close to that observed in complexes **11b**, **12b**, and **13b** (Table 4). In such a conformation, the Na(3) cation is allowed to enter the cavity, binding to the O(1) and O(3) atoms. In agreement with to the presence of a five-coordinated metal, the macrocycles in units B and C display nearly regular cone conformations (Table 4).

The trinuclear nitrido complex **15a**, depending on the nature of the solvent, i.e. $CHCl_3$ and/or the addition of a co-ligand for the alkali metal cation, breaks up into smaller nitrido complexes. Addition of TMEDA to solutions of **15a** led to the formation of **16** (in toluene) and **17** (in $CHCl_3$). Complex **16** maintains the overall structure of complex **11b**, the only difference being the solvation of sodium cations by TMEDA. Its spectroscopic properties (^{1}H NMR, ^{15}N NMR) are very similar (see Experimental Section) to those of **11b**, as is its X-ray analysis, which is given in the Supporting Information.

The ^{1}H NMR spectrum of **17** indicates a 4-fold symmetry calix[4]arene, while the ^{15}N NMR spectrum of the labeled sample displays a singlet at 167.7 ppm (py-d_5) and at 160.9 ppm ($CDCl_3$). Complex **17**, crystallized from chlorobenzene, gave crystals suitable for an X-ray analysis. The structure of the anion is displayed in Figure 7. The dimer possesses a crystallographically imposed C_m symmetry, the mirror plane running through the nitrogen atom. The Nb−N(1) bond distance [1.854(2) Å] is between those observed in **7c** and **11c**, reflecting to a partial double-bond character, while the Nb−N−Nb skeleton is bent [Nb(1)−N(1)−Nb(1)′ = 145.2(1)°]. The O_4 core shows very small tetrahedral distortion (Table 4), so that coordination around niobium should be better described as square pyramidal, with the oxygen atoms from calixarene defining the base and the N(1) atom at the apex. The metal is displaced 0.500(1) Å from the O_4 mean plane, the Nb−N(1) vector forming a dihedral angle of 0.6(2)° with the normal to the plane. The Nb−O bond distances (mean value 1.943(5) Å) are just significantly different from each other and fall in the usual range of values. The macrocycle assumes an elliptical conformation, with the A and C rings being slightly pushed outward and the B and D rings slightly pushed inward relative to the cavity (Table 7).

Recombination of **11a** and **17** in toluene occurred to re-form **15b**, as confirmed by its ^{1}H and ^{15}N NMR spectra in solution and by its isolation in the solid state.

Discussion

The generation of reduced forms of Nb-calix[4]arene (see Scheme 1) required overcoming a number of synthetic difficulties. The first one was the synthesis of the starting material, **1**. Among all the methods applied so far to the synthesis of metallacalix[4]arenes,[8] the most appropriate in the present case is the direct reaction of $NbCl_5$ with the protic form of calix[4]-

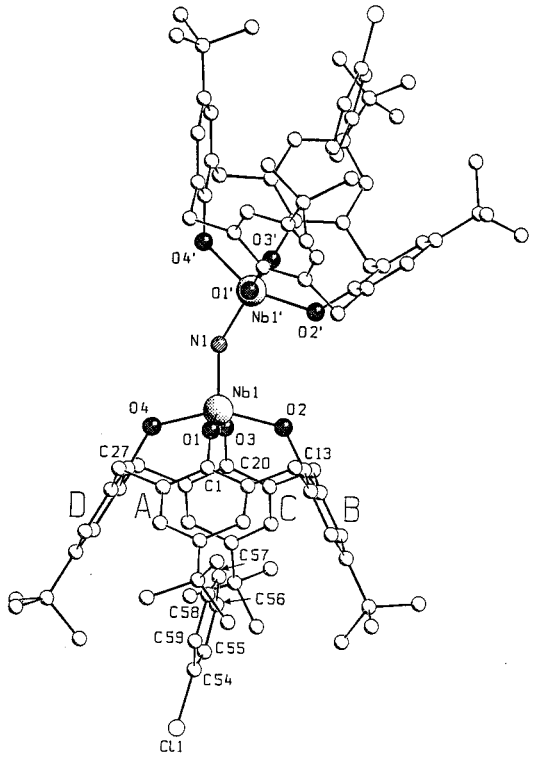

Figure 7. Simplified SCHAKAL view of the anion in complex **17**. Disorder affecting the *tert*-butyl groups of the C and D rings has been omitted for clarity. A prime denotes the transformation $x, 1 - y, z$.

arene in toluene, care being taken to remove HCl completely (see the Experimental Section). Reduction of **1** should be performed in a stepwise manner. The first step is particularly crucial, since it allows one to remove all the Cl^- anions, which can have a negative effect on the subsequent reactions. Although the first step is usually run under nitrogen, the following reduction should be carried out strictly under an argon atmosphere. Reduction of **2** with different alkali metals and a controlled stoichiometry led to the Nb═Nb species, **3**−**5**.[18] According to its ^{1}H NMR spectrum, complex **3** exhibits apparent D_{2h} symmetry in both toluene and THF, while **4** changes from 2-fold symmetry in toluene at low temperature (−40 °C) to 4-fold symmetry in THF. The 4-fold symmetry in the ^{1}H NMR spectrum of **4** in THF appears when the alkali metal cations are removed from the calix[4]arene oxygens by the coordinating solvent.

The electronic structure of the dianion present in complexes **3**−**5** was analyzed using extended Hückel calculations.[32] For this purpose, the calix[4]arene ligands were slightly simplified by replacing the Bu^t groups and the methylene bridges by hydrogens and symmetrizing to a C_{2v} local symmetry, while the geometrical constraints on the O_4 set of donor atoms were maintained according to the structural parameters of **4b**. The same simplifications were used in the cases of the other extended Hückel calculations. The electronic structure of the anion in **3**−**5** was derived from the interactions between the frontier orbitals of two [Nb-calix[4]-$(O)_4$]$^-$ metal fragments and will be referred to from now on as **4**. The frontier orbitals of the [Nb-calix[4]-$(O)_4$]$^-$ fragment are shown on the left in Figure 8 and consist of four low-lying empty metal-based orbitals. The $d_{x^2-y^2}$ orbital, which points more toward the oxygen ligands, is pushed high in energy while the remaining four d orbitals are found within 1 eV. The LUMO is a $1a_1(d_{z^2})$ orbital with the

(32) (a) Hoffmann, R.; Lipscomb, W. N. *J. Chem. Phys.* **1962**, *36*, 2179. (b) Hoffmann, R. *J. Chem. Phys.* **1963**, *39*, 1397.

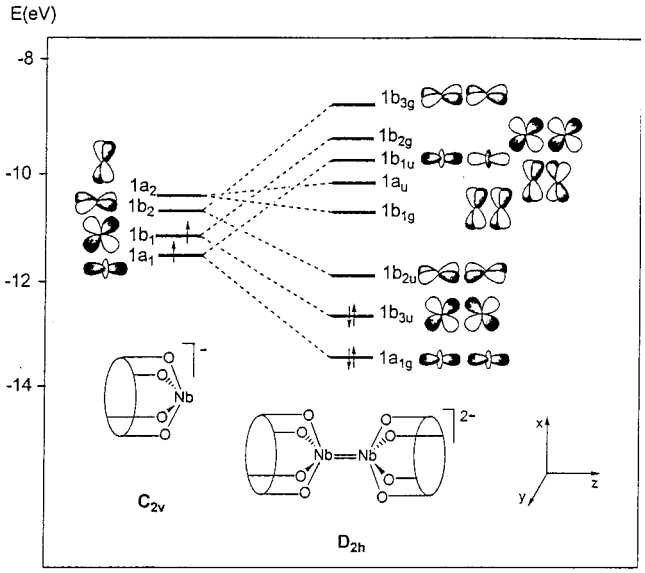

Figure 8. Orbital interaction diagram for **4**.

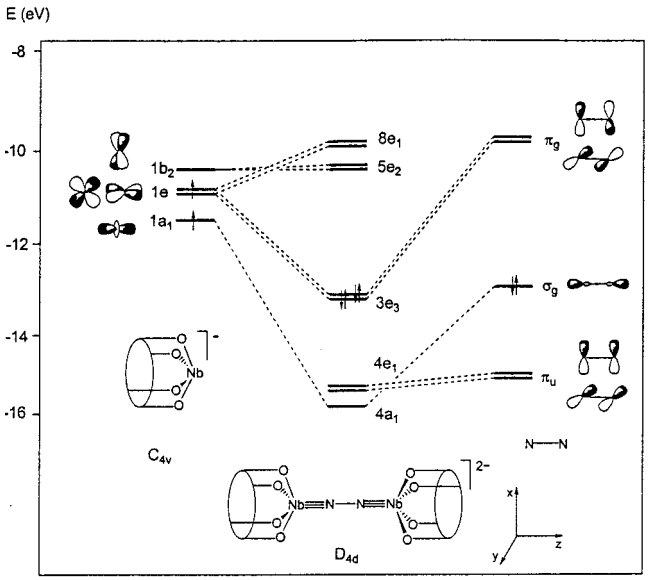

Figure 9. Orbital interaction diagram for **7** with D_{4d} symmetry.

$1b_1(d_{xz})$ and $1b_2(d_{yz})$ orbitals 0.2 and 0.8 eV above, respectively (see Figure 8). Because of the in-plane π interactions with the oxygen atoms, the $1a_2(d_{xy})$ orbital still lies 0.3 eV higher in energy. For such an Nb^{III} fragment with a d^2 electron count, these orbitals are occupied by two electrons, as shown in Figure 8. The interaction between the two [Nb-calix[4]-$(O)_4$]$^-$ fragments is illustrated by the molecular orbital diagram on the right in Figure 8 and shows an Nb−Nb $\sigma^2\pi^2$ configuration, indicating, therefore, metal−metal double-bond character that is consistent with the observed metal−metal distance of 2.659(1) Å.[18] It is worth noting the effect on the electronic structure of the distortion from C_{4v} to C_{2v} local symmetry around the metal shown by the crystallographic data. Indeed, we observe significantly different Nb−O bond distances in the two orthogonal O(1)−Nb−O(3) and O(2)−Nb−O(4) planes, those involving O(1) and O(3) being almost 0.2 Å shorter than those involving the Na^+-bridged O(2) and O(4) (see Figure 1 and Table 2). This distortion reduces the symmetry of the dimer to D_{2h} and causes a significant splitting of the two π orbitals, leading to a singlet ground state instead of the triplet state expected for a D_{4h} dimer. Although, at first sight attributable to the presence of the two bridging alkali metal cations, this distortion is probably electronic in nature and due to a dynamic Jahn−Teller effect as suggested by the ^{1}H NMR studies of **4**. Indeed, the ^{1}H NMR spectrum of **4** in THF shows a 4-fold symmetry, indicating that the alkali metal cations are removed from the calix[4]arene oxygens by the coordinating solvent without inducing any paramagnetism.

As far as the M═M reactivity is concerned, the reactivity of **3**−**5** has very few analogues,[33] the closest one being that of $[W_2(OR)_8]$ containing a d^2−d^2 W═W unit.[34] The major difference from the latter, besides the difference in the metal−metal bond energy, lies in the presence, in the case of tungsten, of strong bridging alkoxo groups. In the case of $[W_2(OR)_8]$,[34a] reactions with C_2H_4, CO, and Ph_2CO occurred preferentially at a single metal center rather than at the M═M double bond and led to a terminal CO, ethylene, and η^2-ketone derivatives. In contrast to those of $[W_2(OR)_8]$, the reactions of **3**−**5** occurred with two distinctive characteristics, namely complete cleavage of the M═M bond and four-electron reduction of the substrates N_2, R_2CO, and RCHO.[25] The nature of the alkali metal cation, which determines the strength of the interaction with the calix-[4]arene oxygens, is a determining factor for the reactivity of **3**−**6** and its dependence on the solvent used. As a matter of fact, we found that the potassium derivative **5** reacts faster than the sodium derivative **4** and that the latter reacts faster than the lithium compound **3**. The significant difference in reactivity among the three Nb═Nb compounds, even in coordinating solvents, can be ascribed to the different degrees of association of the alkali metal cations with the anion in complexes **3**−**5**. The same reactivity is reasonably expected for completely ion-separated ion-pair forms, but this is not the case. In this context, we should mention two other experimental observations: the negligible reactivity of **3** toward dinitrogen in a toluene solution and the very different pathway involved in the reaction of **4a** with dinitrogen in toluene (see below).

It should be emphasized, in the present chemistry, that solvation of the alkali metal cation and the ion-pair nature of the reduced forms can indirectly have relevant effects on the kinetics and the energetics of the reaction. The reaction of dinitrogen led, in the case of **3**−**5**, essentially to the same bis-(metallahydrazone) derivatives, **6**−**8**. Complexes **3**−**5** are diamagnetic both in the solid state and in solution, as confirmed by NMR and EPR analyses. This diamagnetism rules out their dissociation into the monomeric d^2 niobium reactive species. Therefore, the reaction of **3**−**5** would not occur by the conventional mechanism, implying the intermediacy of a mononuclear end-on dinitrogen complex. We are much more in favor of the N≡N bond undergoing a sort of metathesis reaction with the Nb═Nb bond, up to the formation of the hydrazido form, the reaction being reminiscent of **4a** reacting with azobenzene, leading to the terminal phenylimido derivative.[6]

The electronic structure of the dianion in **6**−**8**, hereafter referred to as **7**, was analyzed in terms of the interactions between the frontier orbitals of the two [Nb-calix[4]-$(O)_4$]$^-$ metal fragments and the central N_2 unit. The frontier orbitals of the [Nb-calix[4]-$(O)_4$]$^-$ fragment are shown on the left in Figure 9 and differ from those in Figure 8 because the metal

(33) Casey, C. P.; Carino, R. S.; Hayashi, R. K.; Schadetsky, K. D. *J. Am. Chem. Soc.* **1996**, *118*, 1617.

(34) (a) Chisholm, M. H.; Folting, K.; Lynn, M. A.; Streib, W. E.; Tiedke, D. B. *Angew. Chem., Int. Ed. Engl.* **1997**, *36*, 52 and references therein. (b) Anderson, L. B.; Cotton, F. A.; DeMarco, D.; Fang, A.; Ilsley, W. H.; Kolthammer, B. W. S.; Walton, R. A. *J. Am. Chem. Soc.* **1981**, *103*, 5078. (c) Cotton, F. A.; Falvello, L. R.; Fredrich, M. F.; DeMarco, D.; Walton, R. A. *J. Am. Chem. Soc.* **1983**, *105*, 3088.

fragment has C_{4v} symmetry and the two d_π orbitals are degenerate and constitute the 1e(d_{xz},d_{yz}) set. On the extreme right in Figure 9 are shown, the frontier orbitals of N_2, i.e., the occupied σ_g and π_u and the empty π_g orbitals. The interaction between the two [Nb-calix[4]-$(O)_4$]$^-$ fragments and the central dinitrogen unit is illustrated by the molecular orbital diagram in the central column of Figure 9, which shows two main bonding interactions, i.e., that between the 1a_1(d_{z^2}) and σ_g orbitals and that between the doubly degenerate 1e(d_{xz},d_{yz}) and π_g orbitals. The 1e(d_{xz},d_{yz}) orbitals of the [Nb-calix[4]-$(O)_4$]$^-$ metal fragments are considerably higher, in energy and thus they match quite well with the nitrogen π^* orbitals giving rise to the low-energy 3e_3 orbitals, whose full occupation by four electrons leads to a significant degree of back-donation to the N_2 π^* orbitals (2.18 electrons). The consequent lengthening of the N−N bond is shown by the decrease of the overlap population from 1.18 in free N_2 (with the same N−N bond length as that of **7**) to 0.74. The four-electron reduction of N_2, depicted by the Nb≡N−N≡Nb bonding picture, is consistent with the N−N [1.390(17) Å][3,35] and short Nb−N [1.747(12) Å] bond lengths.[20] In conclusion, the very efficient electron transfer to the N_2 molecule causing the formation of a rather acidic Nb(V) explains the formation of the Nb≡N triple bond, the linearity of the Nb═N−N═Nb skeleton, and the rather long N−N bond ready to be cleaved. It is interesting to compare the [Nb-calix[4]-$(O)_4$]$^-$ fragment in **7** with other metal fragments involved in analogous dinuclear end-on dinitrogen complexes. The [Nb-calix[4]-$(O)_4$]$^-$ fragment has the same $2\pi1\sigma$ frontier orbital pattern[36,37] that characterizes the tris(amido)- and {tris-amido(amine)} metal fragments involved in some recently characterized dinitrogen complexes of group 6 metals with end-on "hydrazido(4−)" $M_2(\mu$-$N_2)$ character.[2a,c,4] In particular, the [Nb-calix[4]-$(O)_4$]$^-$ fragment and the [Mo(N(R)Ar)$_3$] tris(amido) fragments have similar energies for the σ and the two π frontier orbitals and differ from the {tris-amido(amine)} metal fragments, showing a much higher energy for the 1σ(d_{z^2}) orbital, which is destabilized by an axial σ-donor ligand.[37]

Moving from complexes **3**−**5** to complexes **6**−**8**, the alkali metal cation is released from the calix[4]arene oxygens. Once again, we should draw attention to the fact that solvation of the alkali metal cations contributes to the driving force of such reactions. Compounds in Scheme 2 appear with different solvations for the alkali metal countercations, depending on the reaction and crystallization solvents. The high acidity of Nb(V) complexes **6**−**8** is shown by the formation of the Bu^{t}NC adduct **9**, having a C−N stretching vibration moving up to 2206 from 2136 cm^{-1}. The complexation of Bu^{t}NC to the metal strongly affected the structural parameters of the end-on bonded N_2, with a remarkable increase in the Nb−N bond distance [1.810(8) Å], a decrease in the N−N bond distance [1.303(11) Å], and a slight deviation from linearity for the Nb−N−N−Nb skeleton [Nb−N−N = 174.8(9)°].[19b] These variations in the structural parameters were reflected in the absence of N−N bond cleavage when **9** was reacted with sodium metal (see below). This effect is probably due to the energy rise of the d_{z^2} metal orbital upon complexation of Bu^{t}NC, which destabilizes the metal−nitrogen σ interaction. The same effect due to a σ-bonding axial ligand is experienced by N_2 in the dinitrogen complexes of group 6 metals bonded to the {tris-amido(amine)} ligands.[2c] The four-electron-reduced form of dinitrogen in complexes **6**−**8** has been supported by both the structural parameters and the reaction of **7a** with PhCHO, leading to the corresponding azine, PhCH═N−N═CHPh, and the oxoniobium(V) complex **10**.[3c,f,g]

Scheme 6

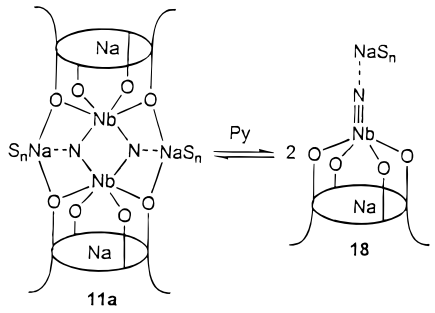

The complete cleavage of the N−N bond to nitride requires two additional electrons under the condition that we keep the Nb≡N triple bond, as confirmed by the absence of any reactivity of **9** with sodium metal. The two additional electrons can be supplied by using either an alkali metal or the starting complex **4a** itself. In the latter case, the formation of nitrides proceeds directly from the reaction of **4a** with N_2 (see below). The solvent is a crucial determining factor in all such reactions. The reduction of **7a** with sodium metal in THF (Scheme 3) gave as the main product a colorless crystalline solid, **11a**, which, however, was isolated from a deep green solution. The latter contains some byproducts which can be very informative regarding the (or one of the) cleavage pathway(s) of the N−N bond. As a matter of fact, when the reaction was carried out in other solvents (see below), it was possible to identify the green component of the solution as a major product of the reaction. Complex **11** has been labeled **a**, **b**, or **c** (Scheme 3) depending on the solvation of the sodium countercations. The complete cleavage of the N−N bonds is confirmed by the structural parameters of **11b**, which has a very long N- - -N separation, while the bent bridging nitrido species has an Nb−N bond distance those of a single and a double bond (Table 2).[26,27] The discrepancy between the 2-fold symmetry of **11a** as revealed by the solid-state structure and its 4-fold symmetry found in solution by ^{1}H NMR spectroscopy in pyridine can be explained by assuming that the equilibrium sketched in Scheme 6 is completely shifted to the right. The oligomerization of metal nitrides[38] and metal arylamides[39] into dimers and trimers is a known phenomenon, though its reversibility seems far less common. The insolubility in nonpolar solvents and the good solubility in pyridine only limit the choice of NMR solvents. Additional support for the dissolution of **11a** in the form of the monomeric species **18** is the chemical shift of ^{15}N in the isotopically enriched sample at +269.4 ppm (reference CH_3-NO_2), which is in agreement with the presence of an Nb≡N triple bond (see below).[10,28] It should also be mentioned that the ^{1}H NMR spectrum of **11a** in solution is surprisingly similar to that of **10**, which is isoelectronic and isostructural with **18**. The transformation of **7** to **11** occurs not only with cleavage of the residual N−N bond but also with a remarkable change in the orientation of the N···N vs the Nb−Nb axis, moving from an end-on to a side-on arrangement, so that the two N atoms undergo a quasi-rotation of 90° upon going from **7** to **11**. To

(35) A compilation of N−N bond lengths in dinitrogen complexes is reported in ref 3j.

(36) Schrock, R. R. *Pure Appl. Chem.* **1997**, *69*, 2197.

(37) Schrock, R. R. *Acc. Chem. Res.* **1997**, *30*, 9.

(38) (a) Chisholm, M. H.; Folting, K.; Lynn, M. L.; Tiedtke, D. B.; Lemoigno, F.; Eisenstein, O. *Chem.−Eur. J.* **1999**, *5*, 2318. (b) Pollagi, T. A.; Manna, J.; Geib, S. J.; Hopkins, M. D. *Inorg. Chim. Acta* **1996**, *243*, 177. (c) Bernaszak-Holl, M. M.; Kersting, M.; Pendley, B. D.; Wolczanski, P. T. *Inorg. Chem.* **1990**, *29*, 1518.

(39) Solan, G. A.; Cozzi, P. G.; Floriani, C.; Chiesi-Villa, A.; Rizzoli, C. *Organometallics* **1994**, *13*, 2572.

Scheme 7

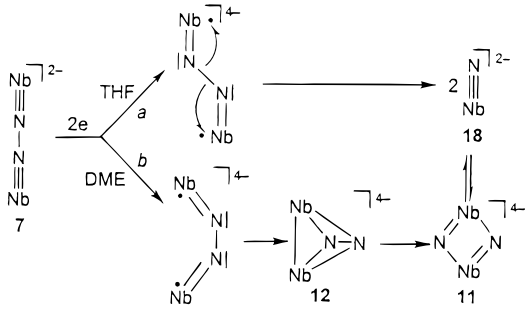

Chart 2

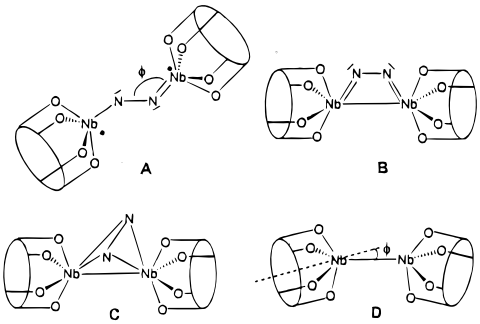

understand the possible pathways from **7** to **11**, we had to determine what happens when two electrons are added to **7**.

Figure 9 shows that the two extra electrons first occupy the $5e_2$ and/or $8e_1$ orbitals, of antibonding character, thereby destabilizing the system. Two different limiting pathways (a and b in Scheme 7) can be hypothesized for the evolution of $[\mathbf{7}]^{2-}$ species. In the first pathway (a), the linear Nb≡N−N≡Nb unit bends to give a trans structure, where each nitrogen has an sp^2 hybridization and one lone pair (A in Chart 2). This zigzag structure then undergoes an N−N cleavage, leading to the monomeric imido species **18**, which dimerizes in the solid state to **11**. This is what we experimentally observed when performing the reduction of **7a** in THF. This process is reminiscent of the thermal cleavage of the N−N bond in the $[\{Mo(N(R)Ar)_3\}_2(\mu\text{-}\eta^1\text{:}\eta^1\text{-}N_2)]$ tris(amido) complex[4] with the same d^3 configuration of the metal and the same end-on linear geometry as in $[\mathbf{7}]^{2-}$. It should be emphasized, however, that the d^3-d^3 Mo−dinitrogen complex is stable at low temperature and, unlike $[\mathbf{7}]^-$, can be isolated and structurally (EXAFS) characterized at −35 °C, giving rise to N−N bond cleavage only upon mild heating.

Pathway b depicted in Scheme 7 gives the alternative sequence leading to **11**. Such a sequence has quite strong experimental support in the isolation of **12** (Scheme 4). The key factor in the successful interception of intermediate **12** was the choice of the reaction solvent. When the reduction of **7** with sodium was carried out in DME, a negligible amount of **7b** as white crystals was detected, along with the formation of deep green crystals of **12** as the major product of the reaction. The role of **12** as one of the possible intermediates in the formation of the nitrido complex has been confirmed by its thermal decomposition to **11c** upon heating in pyridine at 90 °C overnight (Scheme 4). The cis arrangement of the Nb−N−N−Nb unit is probably encouraged by the formation of an Nb−Nb bond (see **B** in Chart 2), which stabilizes the biradical system. Concurrently, the metal−metal bond forces a change in the bonding of dinitrogen from the end-on mode to a $\mu\text{-}\eta^1\text{:}\eta^1$ mode, with the N−N axis still parallel to the Nb−Nb axis. The further rearrangement of N_2 to a $\mu_2\text{-}\eta^2\text{:}\eta^2$ bonding mode, found in complex **12**, has been shown to result in a better interaction with the metal centers.[40] The side-on bonding mode of dinitrogen across two metal ions is no longer rare.[29] The two pathways leading to the N−N bond cleavage are not very different. In both cases, in the preliminary step, the two electrons supplied to **7** give a pair of free-radical-type metals ($d^1\cdots d^1$). In the transoid arrangement, because of the reciprocal disposition of the metals preventing any metal−metal bond and owing to the tendency of the metal to form one σ and two π bonds, the biradical species evolves directly to the formation of the terminal imido derivative **18**.

In the case of pathway b (Scheme 7), the metal−metal (d^1-d^1) bond temporarily stores the two electrons supplied by sodium. Then a facile thermally induced intramolecular electron transfer occurs from the metal−metal bond to the N−N bond with its consequent cleavage. It should be emphasized that the rearrangement of N_2 from the end-on (complex **7b**) to the side-on bonding mode (complex **12b**) occurs without any significant change in the N−N bond distance (1.39 vs 1.40 Å), and thus in the degree of potential reduction of N_2. It is remarkable that the selection of pathways a and b in Scheme 7 can be made by using different solvents, THF vs DME, in the reduction of **7a** with sodium. This fact emphasizes the special role played by solvents in this "bifunctional" chemistry. In addition, the slight difference between the two solvents suggests that the two pathways are probably not so different in energy. Pathway b, leading to a cis bending of the M_2N_2 skeleton and to the formation of a metal−metal bond, was not observed for the analogous d^3 Mo(III) tris(amido) complex,[4] probably because of the high steric hindrance of the N(Bu^t)Ar amido ligands, which prevent close approach of the molybdenum atoms.

The possible evolution of $[\mathbf{7}]^{2-}$ was analyzed using extended Hückel calculations, varying the two Nb−N−N angles θ in both trans and cis depositions. Figure 10 plots the change in the total energy of the complex when the angle θ is decreased and all other geometrical parameters are fixed at their values in **7**. In this figure, the potential curve for cis bending is initially very similar to that for trans bending, both bent geometries showing only a slight energy increase from the linear structure (θ = 180°). However, while the potential curve for trans bending shows a sharp increase for θ lower than 150°, the curve for cis bending shows a maximum and then a minimum at ca. 140°, corresponding to the formation of a metal−metal bond, followed by a sudden increase. This shows that the two proposed pathways are isoenergetic in the initial stages and suggests that the two bent geometries represent essentially transition structures on the pathway toward direct N−N cleavage (trans bending; see below) or metal−metal bond formation (cis bending). In particular, the minimum found in the potential curve around 140° corresponds to the hypothesized dinitrogen complex with the N_2 moiety parallel to the metal−metal axis (see **B** in Chart 2). Pathway a (Scheme 7) passing through a zigzag structure is analyzed here. Since a qualitative correlation diagram for this process has already been published for the analogous d^3 Mo(III) tris(amido) complex,[4] we considered only the total energy profile. For this purpose, we performed extended Hückel calculations on **7**, $[\mathbf{7}]^-$, and $[\mathbf{7}]^{2-}$ with increasingly lengthened N−N distances, from 1.39 to 2.3 Å. At each point along this reaction pathway, we relaxed the Nb−N distance and Nb−N−N angle θ (see **B** in Chart 2), obtaining the total energy profiles

(40) Goldberg, K. I.; Hoffman, D. M.; Hoffmann, R. *Inorg. Chem.* **1982**, *21*, 3863.

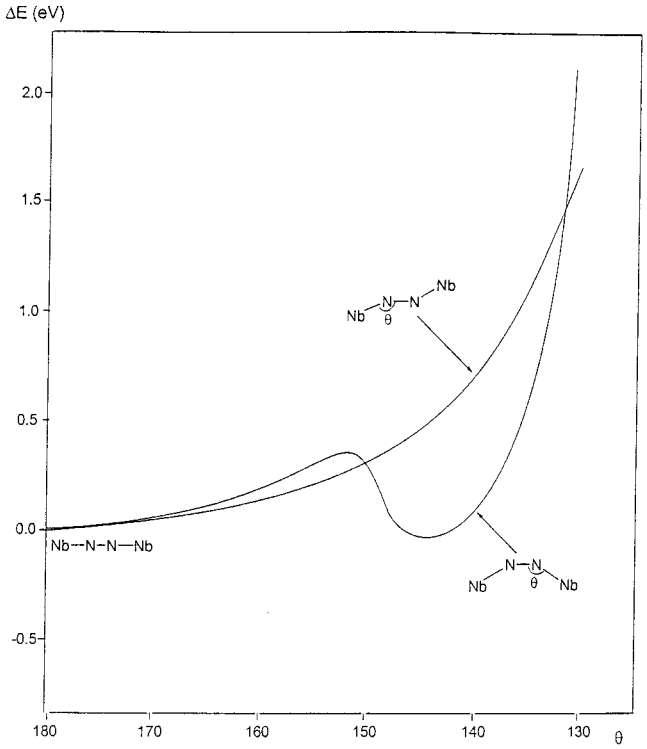

Figure 10. Potential energy curves for cis and trans Nb−N−N−Nb bending of $\mathbf{7}^{2-}$.

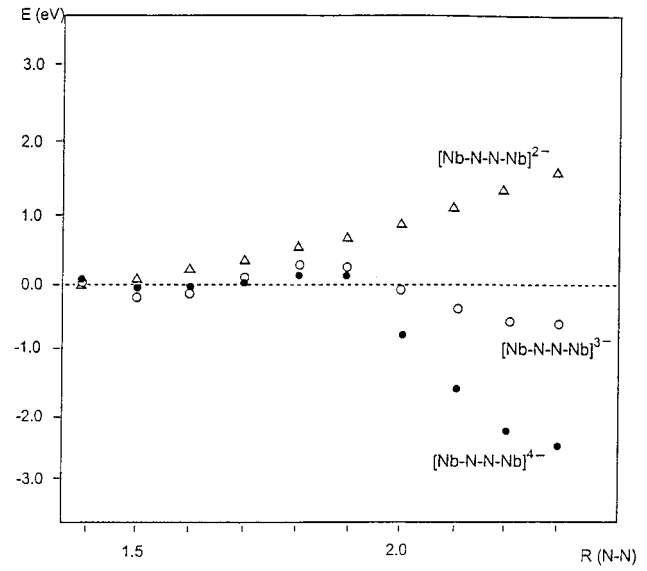

Figure 11. Total energy profiles for the N−N cleavage in **7**, $[\mathbf{7}]^{-}$, and $[\mathbf{7}]^{2-}$.

displayed in Figure 11. The cleavage is endothermic for **7** but slightly exothermic for $[\mathbf{7}]^{-}$ and strongly exothermic for $[\mathbf{7}]^{2-}$, the small energy barriers being 5 and 10 kcal mol^{-1}, respectively. In the proximity of the transition state of $[\mathbf{7}]^{2-}$ (at R(N−N) > 1.8 Å), we found a zigzag structure for the Nb−N−N−Nb unit with Nb−N−N angles of ∼140°. This structure corresponds to an Nb═N̈−N̈═Nb bonding scheme where each nitrogen has an sp^2 hybridization and one lone pair, which allows it to overcome the symmetry-forbidden nature of N−N bond cleavage along a linear trajectory.[4] Although the extended Hückel approach is not suitable for bond energy calculations, these energy profiles clearly indicate that reductive cleavage of the N−N bond is a thermodynamically favorable process with a small energy barrier.

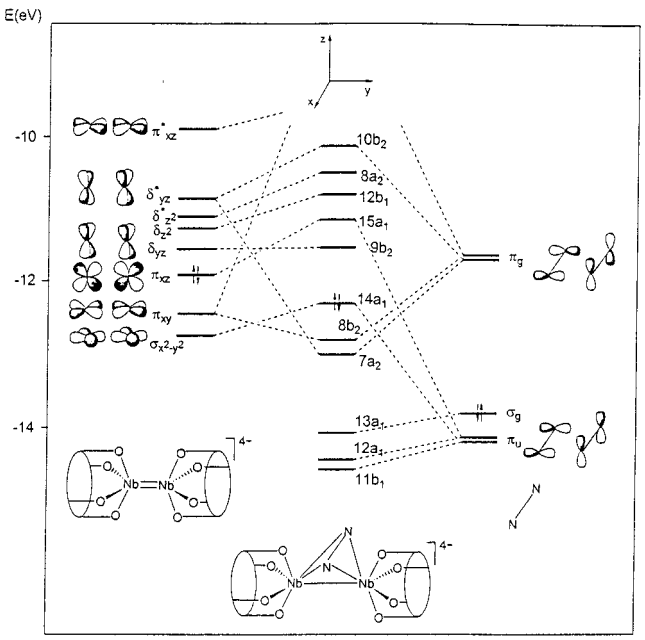

Figure 12. Molecular orbital interaction diagram for **12**.

The evolution along pathway b in Scheme 7 was then analyzed. The extended Hückel calculations were performed, first, on a simplified model of **12** (see **C** in Chart 2). To maintain a C_{2v} symmetry, we symmetrized the two Nb(calixarene) units, thus disregarding the presence of a bridging oxygen and using the geometry of the undistorted niobium calixarene fragment. The electronic structure of **12** is analyzed in terms of the interactions between the frontier orbitals of the dinuclear [Nb-calix[4]-$(O)_4]_2^{4-}$ unit and the N_2 moiety. The frontier orbitals of the dinuclear unit are built up as reported for **4** (Figure 8) and are displayed on the left in Figure 12. Two [Nb-calix[4]-$(O)_4]^{2-}$ fragments are brought close together in D_{4h} symmetry, and the resulting orbitals are essentially the in- and out-of-phase combinations of the orbitals of [Nb-calix[4]-$(O)_4]^{2-}$, as outlined above. In the next step, the niobium calixarene groups are bent backward, maintaining a local C_4 symmetry (see **D** in Chart 2), and the angle ϕ is optimized, thus reducing the symmetry from D_{4h} to C_{2v}. Calculations performed on this model of **12** with geometrical parameters taken from its X-ray structure (Figure 4) and with optimization of the bending angle θ show that the energy is only slightly affected by the cis bending. We therefore consider the most symmetric D_{4h} dinuclear fragment, which simplifies the discussion and is also consistent with the X-ray structure of **12**, in which the local C_4 axis of the undistorted niobium calixarene (see moiety **A** in Figure 4) is parallel to the Nb−Nb axis. The interaction diagram, presented in Figure 12, shows two main stabilizing interactions between the metal fragment orbitals of π_{xy} and δ^*_{yz} character and the two z and x components of the antibonding π^* orbitals of N_2, **E** and **F**, respectively, in Chart 3. These interactions lead to a significant degree of back-donation, as reflected in the high occupancy of the N_2 π^* orbitals, 1.06 and 1.16 for the a_1 and b_2 components, respectively. The effect of such back-donation and of the simultaneous forward donation from the N_2 π orbitals to the metals is to weaken the N−N bond, as shown by the decrease in the overlap population from 1.18 in free N_2 to 0.75, in agreement with the observed extreme N−N bond length [1.403-(8) Å]. It is worth noting that the [Nb-calix[4]-$(O)_4]^{2-}$ fragment is isolobal with the $[(CO)_3Co]$ fragment, which gives rise to several stable μ-η^2:η^2-acetylene complexes[41] and has been

Chart 3

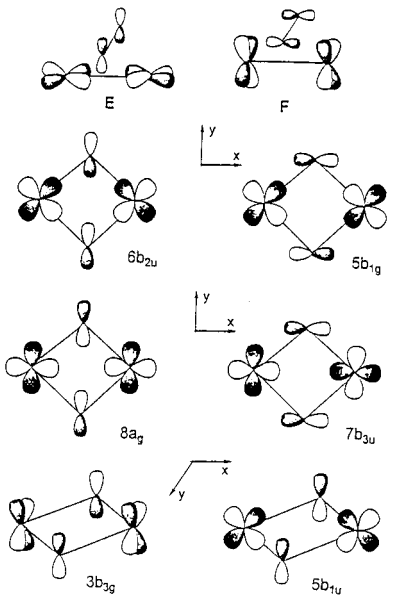

predicted to form stable μ-η^2:η^2-N_2 complexes on the basis of an extended Hückel study.[40]

The relationship between **12** and **11** was analyzed by the procedure we have used thus far. For this purpose, **11** was simplified, though using its structural parameters, to a D_{2h} geometry. The valence orbital levels of **11** are shown on the right in Figure 13. The six highest doubly occupied molecular orbitals represent essentially the interactions of $2p_x$ and $2p_y$ orbitals of the bridging nitrogen atoms with the appropriate metal orbital in-phase or out-of-phase combinations in the metallacycle plane *xy* $6b_{2u}$, $5b_{1g}$, $8a_g$, and $7b_{3u}$ (see Chart 3) and the analogous π interactions of the $2p_z$ nitrogen orbitals with the appropriate metal orbital combinations $3b_{3g}$ and $5b_{1u}$ (see Chart 3). These interactions give rise to the four niobium−nitrogen σ bonds and the two delocalized π bonds of the metallacycle moiety, respectively, resulting in a species of relatively high stability. Indeed, **11** has been found to be almost 100 kcal mol^{-1} lower in energy than **12**. Even with account taken of the extended Hückel deficiency in estimating bond energies, this result indicates that the cyclic nitrido species is very stable and constitutes the "thermodynamic sink" of $[\mathbf{7}]^{2-}$.

At this stage, it should be emphasized that, according to the detailed discussion outlined above, the two pathways a and b in Scheme 7 result in different nitrido species, **18** and **11**, respectively, as primary products, which, however, are in equilibrium according to Scheme 6. The complete picture of **11** and **12** allows one to follow the conversion of **12** into **11**. This process formally involves the cleavage of Nb−Nb and N−N σ bonds and the formation of two Nb−N π bonds, delocalized over the entire Nb_2N_2 metallacycle. A molecular orbital correlation diagram (built in C_{2v} symmetry, although on the right we report the complete D_{2h} symmetry labels for the valence orbitals of **11**) has been calculated for this process and is illustrated in Figure 13. First of all, we note that the high-lying empty orbital of the side-on dinitrogen complex ($10b_2$, describing the NN σ* orbital) correlates, via an avoided crossing, with the HOMO of the cyclic nitride ($6b_{2u}$) and at the same time the HOMO of the side-on complex ($14a_1$, describing essentially the metal−metal bond) correlates with an empty orbital of **11** ($9a_g$). Therefore, the N−N bond cleavage is a symmetry-forbidden process and is expected to show a sizable energy barrier despite the much higher stability of the bond-cleaved product **11**. This result is consistent with the relative thermal stability of **12**, which converts to **11** only when heated above 90 °C. The crossing of the $14a_1$ and $10b_2$ orbitals can be formally seen as a two-electron shift from the filled Nb−Nb σ orbital ($14a_1$) to the empty N−N σ* orbital ($10b_2$), giving an intuitive interpretation of the intramolecular metal to nitrogen electron transfer and the simultaneous N−N bond cleavage. The two electrons of the high-energy $14a_1$ HOMO are, in principle, available not only for the intramolecular electron transfer to dinitrogen but also for an intermolecular redox process in which **12** undergoes a two-electron oxidation, which may cause an Nb−Nb bond cleavage, leaving the dinitrogen unit unchanged.

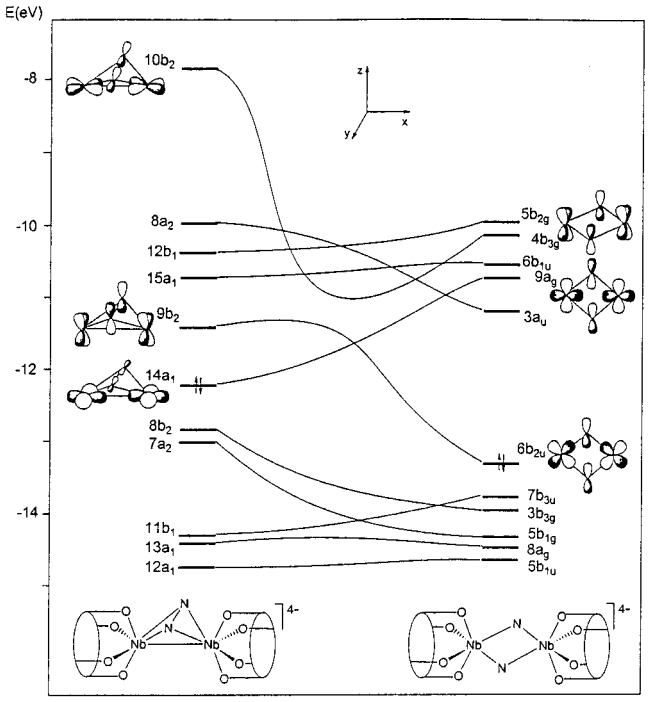

Figure 13. Molecular orbital correlation diagram for the conversion of **12** to **11**.

Such a possibility has been investigated in the reaction of **12** with pyO or O_2 (see Scheme 4), leading to **13**, where an oxo group is inserted between the two metal ions at the expense of the two electrons originally stored in the Nb−Nb bond. The N−N bond is maintained with a μ-η^2:η^2 bonding mode in complex **13**, though significant changes in the structural parameters of the Nb_2N_2 core occur. The lengthening of the N−N bond from 1.403(8) to 1.424(5) Å parallels the shortening of the Nb−N bonds from 2.120(9) (average) to 2.054(5) Å. The increase in the oxidation state of the metal strengthens the interaction of the metal with nitrogen and weakens the N−N bond. A reaction further emphasizing how the two electrons stored in the Nb−Nb bond are available for transformations other than the cleavage of the N−N bond is the formation of **14** upon heating **12** in the solid state. In this case, the two electrons stored in the Nb−Nb bond were made available for cleaving a C−O bond of the calix[4]arene. The reaction led to the insertion of an oxo group between the two Nb ions and the formation of a direct Nb−C bond between the metal and the calix[4]arene moiety. This type of deoxygenation of one of the phenoxo groups[30] was reported to have very little effect on the bonding mode of the dinitrogen unit. This result is particularly interesting, since it offers the possibility of using the two electrons stored in the Nb−Nb bond in **12** for reductive binding

(41) Hoffman, D. M.; Hoffmann, R.; Fiesel, C. R. *J. Am. Chem. Soc.* **1982**, *104*, 3858 and references therein.

Scheme 8

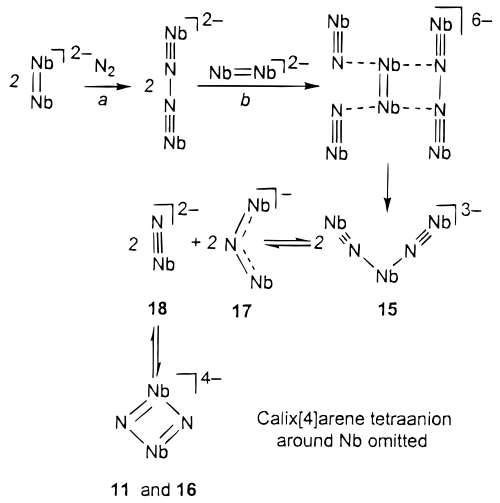

of other substrates while maintaining dinitrogen in its reduced state. There is a further implication from the thermally induced transformation of **12a** into **14a**. The difference between the thermal rearrangements of **12a** in solution (py) and in the solid state, leading to **11c** and **14a**, respectively, emphasizes once more the role of the solvent in this chemistry.

At this stage of our investigation, we pursued the idea of performing the six-electron reduction of dinitrogen using exclusively the active species **4a**, without the help of any additional reducing agent, such as alkali metals. We found that the absorption of dinitrogen by **4a** in toluene, instead of polar coordinating solvents (THF, DME), yielded the trinuclear nitrido complex **15a**, whose structure was clarified by an X-ray analysis (Figure 6) of the solvated form **15b**. In the preceding and in the Experimental Section, we reported how **15a** splits into complexes **16** and **17**. This mechanism has been fully characterized, including confirmation by X-ray analysis. The major focus at this stage is the genesis of **15**, and then those of **16** and **17**. The assumption is that the preliminary stage in the reaction of **4a** with N_2 leads to the formation of **7**, regardless of the reaction solvent. We believe that this reaction is followed in toluene by the further reduction of the metallahydrazone **7** by the excess of the reducing agent **4a** (Scheme 8). This hypothesis is supported by the reaction between **4a** and **7a** in toluene, leading to **15a**, and requires that the solvent employed in the reaction between **4a** and N_2 discriminate between the rates of steps a and b in Scheme 8. The former reaction should be much faster than the second one in THF or DME, while the reverse should be true in a noncoordinating solvent such as toluene. Therefore, by choosing the appropriate solvent, we can accomplish either the four-electron (THF or DME) or the six-electron (toluene) reduction of dinitrogen using the Nb═Nb functionality.

What is the reason for this discrimination by the reaction solvent? The reaction of **4a** in toluene occurs, very probably, on a species which is either different from **4a** in THF or DME or present to a much less extent. The difference in the ^{1}H NMR spectra of **4a** in the two solvents is also remarkable, since we move from a C_{2v} type of symmetry for the calix[4]arene moiety in toluene at low temperatures to a C_{4v} symmetry in THF. The conclusion is that the active species reacting with N_2 is preferentially the alkali metal ion-free dianionic species [{*p*-Bu^t-calix[4]-(O)$_4$}$_2$(Nb═Nb)]$^{2-}$. This hypothesis is additionally confirmed by the much slower rate for the reaction of **3** with N_2 in THF and by the absence of any reactivity of **3** with N_2 in toluene. Therefore, toluene not only slows down the reaction

Scheme 9

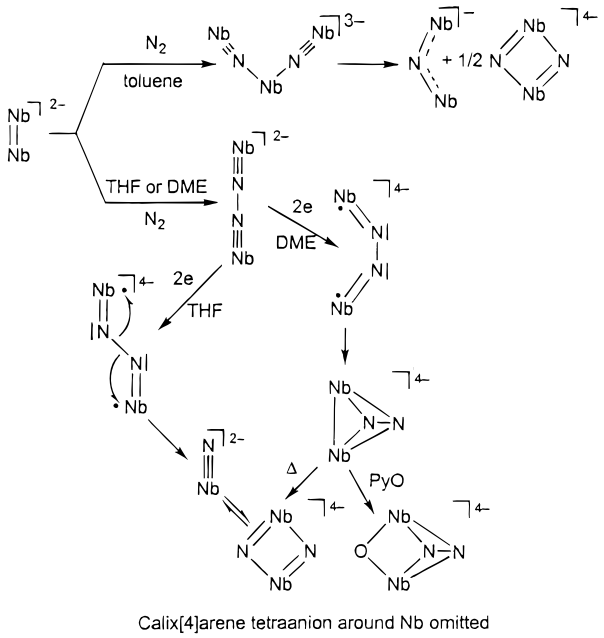

of **4a** with N_2 but also favors the reaction of **4a** with **7a** (step b in Scheme 8). The latter reaction was not observed in THF.

It is plausible to assume that the oxidative addition of the N−N bond in the anionic complex **7a** (step b in Scheme 8) is much more likely to occur at the neutral tight ion pair (toluene) rather than at the anionic form (THF) of **4a**. The weak σ bonding of the two cis nitrides to Nb(1)A in **15b**, in addition to the steric congestion around Nb(1)A, explains the intrinsic lability of **15** and its dissociation into **16** and **17** assisted by an appropriate solvent and favored by the presence of ligands on the alkali metal cations. We can use the same arguments for supporting the series of equilibria sketched in Scheme 8.

Further experimental support for the relationship between the various nitrido species in Schemes 5 and 8 is the reaction between **11a** and **17** in toluene, re-forming **15b**. It should not be surprising that, depending on the solvent and other ligands usable for the alkali metal cations, metal−nitrido aggregates different from those in Scheme 8 could be isolated from the same precursor **15**.

There was a long debate in the early literature regarding the metal-assisted reduction of dinitrogen producing, upon hydrolysis of the reaction mixture, hydrazine and ammonia in different ratios depending on the reaction conditions.[1d,7] The major question was whether ammonia arose from hydrazine disproportionation or from an independent route. The results outlined above regarding the effect of a solvent on the rates of steps a and b in Scheme 8 provide an alternative significant explanation. Under conditions where step a is by far the faster step, the system would produce upon hydrolysis hydrazine exclusively. In the case where step b is the faster step, only ammonia will be detected. For comparable rates of steps a and b, a mixture of N_2H_4 and NH_3 is expected to form in a ratio depending on the reaction conditions.

Conclusion

This paper reports a number of novelties in the metal−dinitrogen chemistry scenario. For the first time, it has been shown that the active species in the reduction of N_2 is a very reactive M═M functionality and that an ancillary ligand containing exclusively oxygen donor atoms can be successfully

employed. The presence of alkali metal ions in the active bifunctional species magnifies the role of the solvent in dinitrogen reduction assisted by transition metal complexes. In particular, the solvent allows one to select either the four- (THF or DME) or the six-electron (toluene) reduction of dinitrogen to hydrazine or ammonia, respectively. In the former case, a fine-tuning of the solvent (DME vs THF) drives the ultimate two-electron reduction of N_2 to nitride through two different pathways, with the interception of key intermediates. Particularly relevant in this context is the rearrangement of the end-on to the μ-η^2:η^2 bonding mode of dinitrogen over a metal−oxo surface modeled by the Nb-calix[4]arene fragment. A comprehensive summary of the different stepwise pathways leading to the reduction of dinitrogen to nitrides is given in Scheme 9.

Acknowledgment. We thank the Fonds National Suisse de la Recherche Scientifique (Grant No. 20-53336.98), Action COST D9 (European Program for Scientific Research; OFES No. C98.008), and the Fondation Herbette (Université de Lausanne) for financial support.

Supporting Information Available: ORTEP drawings, text describing the X-ray data collections and structure solutions and refinements, and tables giving crystal data and structure refinement details, atomic coordinates, isotropic and anisotropic displacement parameters, and bond lengths and angles for **4b**, **7c**, **11b**, **12b**, **13b**, **15b**, and **17**, ORTEP drawings for **9b**, **14b**, and **16**, tables giving crystal data and structure refinement details, atomic coordinates, isotropic and anisotropic displacement parameters, and bond lengths and angles for **16**, and tables giving bond lengths and angles for **9b** and **14b** (PDF). This material is available free of charge via the Internet at http://pubs.acs.org.

JA9943288